Fabrication and Wettability Characterization of Electrospun Fibrous Nylon 6/Silica Nanocomposites

by

Yu Chen

A thesis submitted in partial fulfillment of the requirements for the degree of

Master of Science

Department of Mechanical Engineering

University of Alberta

Abstract

Electrospinning is a simple and versatile method to fabricate polymeric nanofibers and nanocomposite fibers for a wide range of applications. Electrospun Nylon 6 nanofiber mats have been used in tissue engineering, filtration and protective clothing. Silica nanoparticles are a type of popular reinforcements for electrospun fibrous nanocomposites due to its tunable size and biocompatibility. However, electrospun Nylon 6 nanofibers and silica nanoparticles were not studied together before. Therefore, Nylon 6/silica nanocomposite fibers are studied in this thesis.

Firstly, the fabrication process is developed. More specifically, the effect of Nylon 6/formic acid concentration and silica weight fraction on the solution viscosity and the properties of the end product is studied. In microscopic view, scanning electron microscope was used to characterize the morphology and dimensions of the nanofibers. It was found that the average fiber diameter increased significantly with the increase of Nylon 6 concentration and slightly with the rise of silica weight fraction. Also, when silica weight fraction exceeds a critical value, silica nanoparticles start to agglomerate and silica beads appear from time to time. In macroscopic view, surface roughness and porosity of the mats were measured. The porosity remains unchanged while surface roughness increased by increasing silica weight fraction and decreasing Nylon 6 concentration.

In the applications such as filtration and tissue engineering, wettability is a very important surface property. Therefore, after the development of the fabrication process, the change of the mats' wettability with respect to the morphology of the electrospun nanocomposites was investigated. Both the equilibrium water contact angle and the dynamic water contact angle were studied. For pristine Nylon 6 nanofiber mats, the equilibrium contact angle was

increased with the increase of Nylon 6 concentration. The reason is that higher Nylon 6 concentration gives higher average fiber diameter, which results in lower surface roughness. On the other hand, the dynamic water contact angle curves are similar for the mats made from solutions with different Nylon 6 concentration. When silica nanoparticles are reinforced, the variation of equilibrium contact angle is complicated since silica nanoparticles are hydrophobic while the particles also increased the surface roughness of the nanofiber mats. It can be concluded that the surface roughness played a more important role than the particles' hydrophobicity. Dynamic water contact angle is significantly changed by the silica addition. The water drops on the 9% silica reinforced mats were absorbed much quicker than those on pristine Nylon 6 nanofiber mats.

Preface

A version of Chapter 2 of this thesis will be submitted to Journal of Engineered Fibers and Fabrics as a journal publication. The authors of the publication are Yu Chen, Prashant Waghmare, and Cagri Ayranci, and the title is "Fabrication and Characterization of Electrospun Mats of Nylon 6/Silica Nanocomposite Fibers". The work included in this chapter represents the fabricating, characterizing and results interpretation done by me under the guidance of Dr. Ayranci and Dr. Waghmare

A version of Chapter 3 of this thesis will be prepared for submission to a journal following the submission of this thesis. The authors of the publication are Yu Chen, Cagri Ayranci and Prashant Waghmare, and the title is "Tunable Wettability of Electrospun Fibrous Nylon 6/Silica Nanocomposites". The work included in this chapter represents the attempts to achieve tunnable wettability of Nylon 6/silca nanocomcosipte mats done by me under the guidance of Dr. Waghmare and Dr. Ayranci

Acknowledgements

First of all, I would like to express my sincere gratitude to my supervisors Dr. Cagri Ayranci and Dr. Prashant Waghmare for their continuous support in my research. Their patience, motivation, enthusiasm, and immense knowledge helped me in all the time of research and writing of this thesis. Also, I would like to thank Dr. Mark McDermott for being my defense examiner and provide me with valuable suggestions.

Secondly, I would like to thank my girlfriend, Xinyuan He for her support, encouragement and accompany during the past two years of study. I cannot overcome all the hardships and difficulties in research without her.

Last but not the least, I would like to thank my family, my parents and my grandparents, for their encouragement and financial support during my study in the last two years. Thank you for giving birth to me at the first place, providing me with good education and supporting me spiritually throughout my life.

Contents

List of Tables

List of Figures

Chapter 1

Introduction

1.1 Basics of Electrospinning Process

1.1.1 Background and History of Electrospinning

Natural and artificial polymeric fibrous materials are widely used for clothing, furnishing, electronics, and engineering[1]. In the last two decades, polymeric nanofibers have drawn much attention due to their superior properties including high surface-to-volume ratio, good mechanical performance and flexibility in the micro-/nano- structures[2]. Various techniques can be used to fabricate polymeric fibers and nanofibers including drawing[3], self-assembly[4], and electrospinning[5]. Electrospinning is widely used to produce polymeric nanofibers due to its simplicity and great flexibility[6].

The first time that electrostatic force was use to overcome surface tension of the liquids can be dated back to 1882[7]. In 1902, John F. Cooley was able to spray liquid drops with high intensity electrical field[8]. In 1934, Anton Formhals patented the process and its apparatus that could make artificial filaments out of cellulose acetate/acetone solution with the help of high intensity electric field[9]. This is considered as the first electrospinning setup in history. Formhals refined his techniques many times to overcome the drawbacks in his first patent[10]. However, due to the slow production rate and limited characterization techniques, electrospinning remained unnoticed for decades[11]. In 1995, the research interests of electrospinning was revoked by Doshi and Reneker[12] and since then, the number of publications on electrospinning increases every year [13].

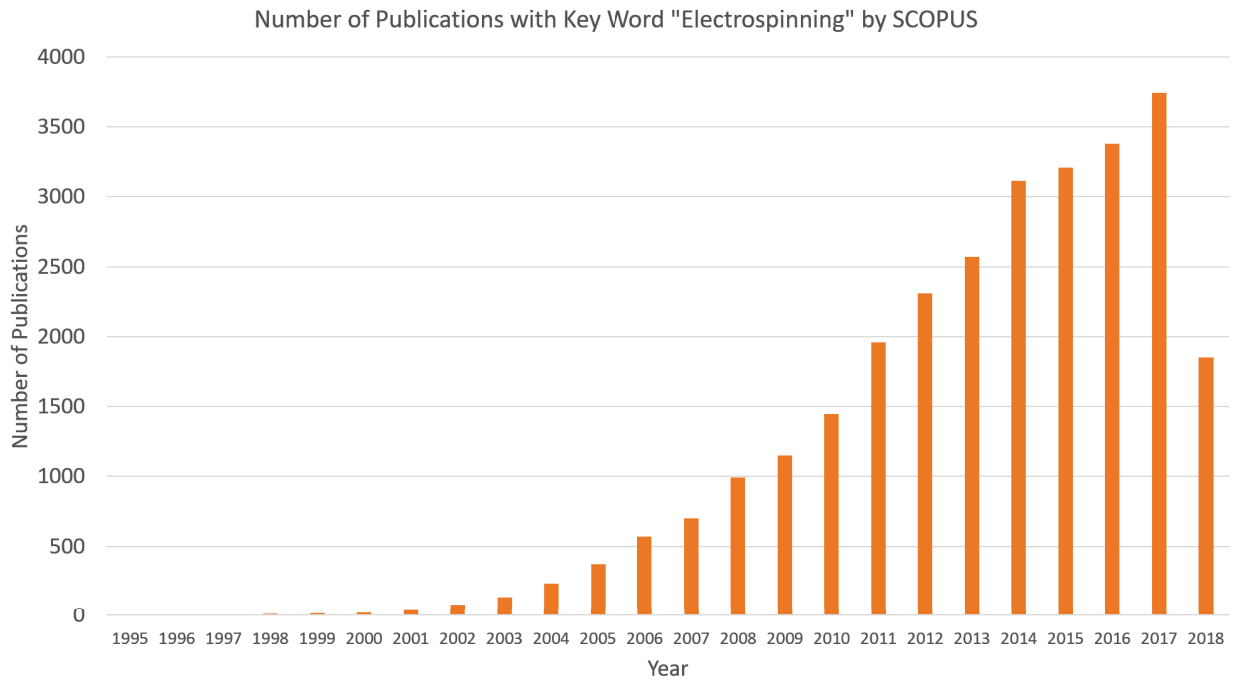

Figure 1.1: Number of publications with key word "Electrospinning" from 1995 to 2018 in SCOPUS Database

1.1.2 Electrospinning Process and Applications

In the electrospinning process, ultrathin polymer nanofibers with average diameter ranging from several micrometers to tens of nanometers can be fabricated[10]. As can be seen in Figure 1.2, the electrospinning setup consists of three main components which are controlled solution feeding component, high voltage generator and grounded collector[7]. First of all, the polymer material is dissolved in the solvent to form a polymer solution and fed into the syringe connected to a blunt needle. Then the syringe and needle that contains the polymer solution is placed on a syringe pump as the controlled solution feeding component. The positive electrode of the high voltage generator is clamped on the needle tip and the ground electrode is connected to the collector. The collector is covered with aluminum foil or a different substrate to ensure perfect grounding and it also makes the electrospun samples removable from the collector.

The electrospinning process is also illustrated in Figure 1.2. When a droplet of polymer solution is pushed out from the needle tip, its shape is governed by the balance between surface tension and the gravitational force. When the intensity of the electrical field between the needle tip and collector reaches a critical value, the repulsive electric force is high enough

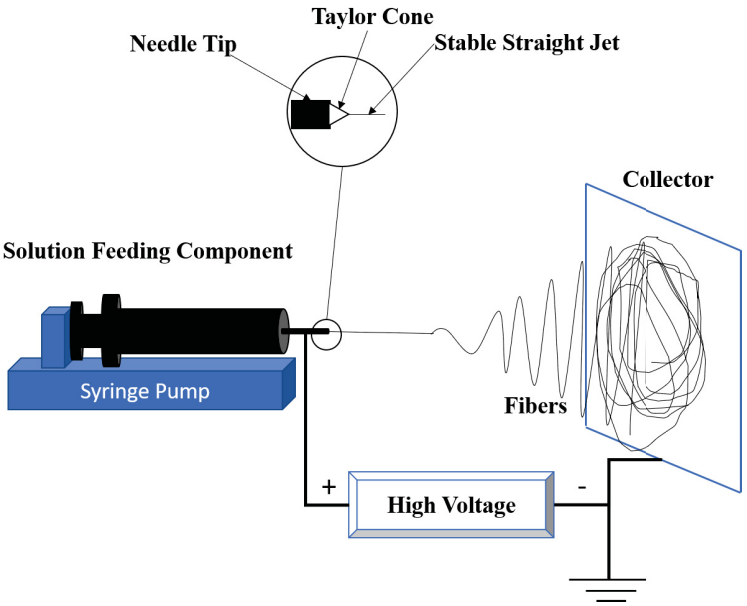

Figure 1.2: Schematic of Electrospinning Setup

to overcome the surface tension of the solution drop at the needle tip, thus a solution jet is ejected towards to grounded collector[12]. In the meantime, a cone shape with half angle of 49.3° is formed[14]. It is called Taylor Cone (see Figure 1.2) which is named after Sir Geoffrey Ingram Taylor and it is independent of the solution properties[15]. After the formation of Taylor Cone, the solution jet travels for a straight trajectory and then undergoes several stages of bending instabilities, which results in the whipping phenomenon, as is shown in Figure 1.2. During the entire flying process, the volatile solvent evaporates and the polymer experiences an elongation[11]. Therefore, the polymer material reaches the grounded collector in the form of fibers with extremely thin diameter and they are randomly distributed on the grounded collector[16].

As can be seen in Figure 1.3, the product of electrospinning is a non-woven nanofiber membrane. Therefore, they can be used in a wide range of applications[2]. Electrospun poly(vinyl alcohol) (PVA) can be used as cell culture scaffolds[17]. Electrospun polyvinylidene fluoride/polydiacetylenes (PVDF/PDAs) has good piezoelectric responses and is a promising candidate for many sensor applications[18]. Polytetrafluoroethylene (PTFE) was successfully electrospun and used as a corrosion resistant layer on the aluminum alloy[19].

Polyamide 6 (PA6, a.k.a. Nylon 6) is one of the most widely used in clothing and textile industry. In the field of electrospinning, the Nylon 6 nanofiber mats are widely used in tissue

(a) Macroscopic View

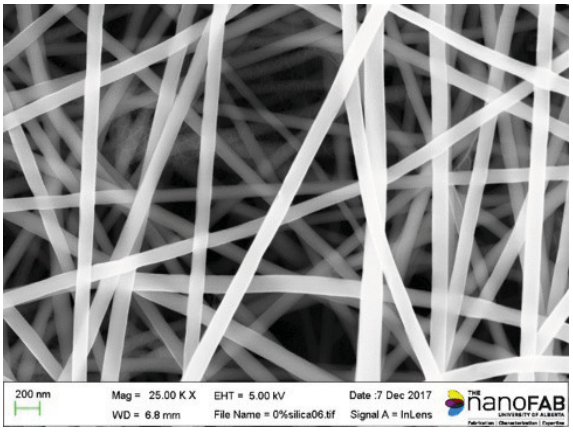

(b) Microscopic View

Figure 1.3: Electrospun Nylon 6 nanofiber mats

engineering, filtration and protective clothing[2][20].

1.1.3 Electrospinning Parameters

As can be seen in the setup of electrospinning in Figure 1.2, the electrospinning parameters can be divided into three categories, which are solution properties, processing parameters and environmental factors[7]. Environmental factors include temperature, relative humidity, atmospheric pressure, air flow, etc[11]. Processing parameters, including applied voltage, flow rate, needle-to-collector distance, needle diameter, are very important and controllable in electrospinning process[14]. They are highly related and usually optimized during the electrospinnig procedure. For example, the applied voltage and needle-to-collector distance determines the intensity electric field and the flow rate should match the intensity of the electric field to form a stable Taylor Cone[15]. The most important parameters are the solutions parameters, including viscosity. solution conductivity, solvent volatility and surface tension[21]. If the viscosity is too high, the electric force will not overcome the surface tension to form a jet, however, if the viscosity is too low, the fibers will have some defects or electrospraying will occur[22]. Solvent volatility is also crucial to the successful electrospinning since the solvent needs to evaporate before the jet hits the collector, otherwise the residual solvent will ruin the existing nanofibers on the collector.

1.2 Wettability

1.2.1 Definition of Wettability

In the above-mentioned applications such as tissue engineering, filtration and protective clothing, wettability is one of the most important properties that needs to be controlled. Wettability is used to describe how a liquid could remain contact with a solid surface and it is a representation of the surface energy [23]. It is determined by the interfacial free energies of the solid, liquid and air [24]. In this project, distilled-water is used as the liquid since in the applications, the water wettability is what the end-users and researchers most interested in. The water contact angle is frequently used to quantitatively describe the water wettability of a solid surface and it is geometrically defined as the angle between the solid surface and the tangential line of the liquid profile, as is shown in Figure 1.4 [25].

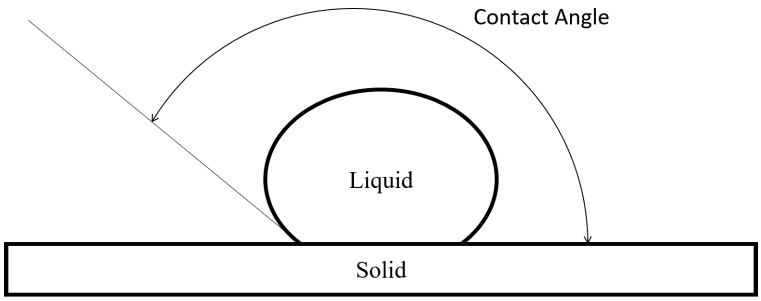

Figure 1.4: Definition of Contact Angle

Usually, there are four types of wetting behaviour between a solid and liquid, namely complete wetting, partially wetting, partially non-wetting and complete non-wetting, as can be seen in Figure 1.5. They are categorized based on the equilibrium contact angle values. As is depicts in Figure 1.5, when the surface tension of the liquid is lower the surface free energy of the solid, the contact angle will be less than 90° and the surface is defined as a hydrophilic surface[24]. On the contrary, when the surface tension of the liquid is higher than the surface free energy of the solid, the non-wetting behaviour will be shown and the contact angle will be higher than 90°[24]. In this case, the surface is defined as a hydrophobic surface.

There is another important information that is worth to be mentioned here. For porous materials, its wetting behaviour is slightly different. Based on Cassie-Baxter's and Wenzel's model, the pore structure of a surface will enhance its original wettability[26, 27]. In details,

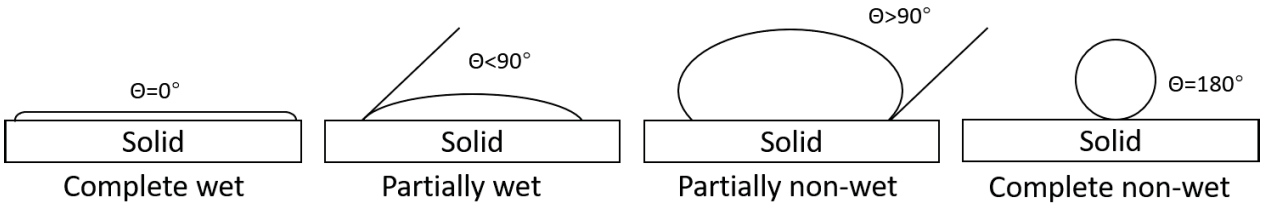

Figure 1.5: Four types of wetting behavior between solid and liquid in the air

the pores on a hydrophobic material will trap some air on the surface so that the contact angle of the hydrophobic surface is increased. On the other hand, the contact angle of hydrophilic surface will decrease since the pores allow more water to be contact with the surface. Another interesting phenomenon is the imbibition process of a water droplet on a porous hydrophilic surface. When a water droplet is deposited on a porous hydrophilic surface, the contact angle will keep decreasing and equilibrium state will never reach since the hydrophilic porous surface will constantly absorb the water droplet[28]. The imbibition process will also be discussed in this thesis since electrospun nanofiber mats is a type of material with high porosity.

1.2.2 Photonic Contact Angle Measurement and Experimental Setup

There are usually two main groups of contact angle measurement techniques: the direct photonics method and the indirect force method[29]. In this project, a direct photonics based measurement system (DSA 100E, KRÜSS GmbH - Germany) along with video and image processing software (ADVANCE, KRÜSS GmbH - Germany) is used to measure and analyze the contact angle of the electrospun mats.

The photonic Drop Shape Analyzer DSA 100E is shown in Figure 1.6 and its main components are briefly illustrated in Figure 1.7. The main components of the system is briefly introduced in the following:

Figure 1.6: DSA 100E

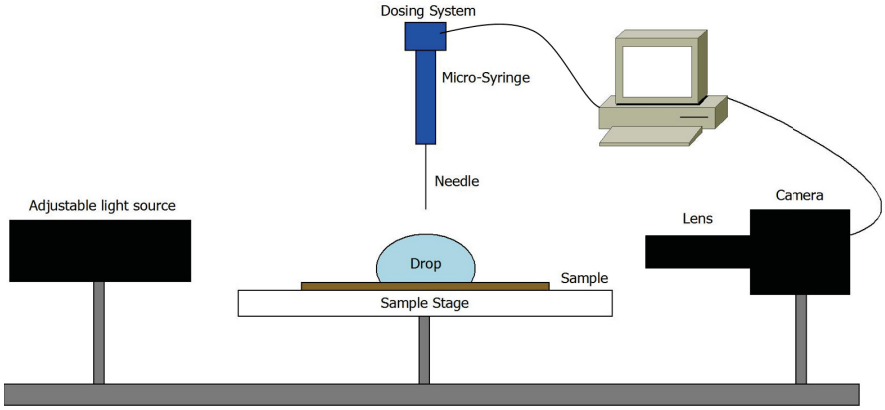

Figure 1.7: Brief illustration of DSA 100E contact angle measurement setup

- **Light source:** The light source is used to provide enough light for imaging. Also, the light intensity of the light source is adjustable to produce a fine image.

- **Camera and lens:** The camera and the lens system are the most important parts of this system. The lens system is optical zoom lens in order to focus on the drop and make it large enough for the data extraction. A high-resolution real-time camera is installed here to capture not only the equilibrium contact angle, but also the drop spreading behavior.

- **Sample stage:** The sample stage is used to place the testing sample. It is adjustable accurately in x, y and z directions to make the drop in the center of image.

- **Dosing system:** A dosing system is used to deposit a certain volume of drop in this measurement system.It consists of a syringe clamp, a micro-syringe and a needle to accurately deposit the liquid drop. It is numerically controlled by the computer.

- **Computer:** The computer is used to acquire the image from the camera and process the image to derive the contact angle value. It is also used to control the dosing system.

1.3 Nylon 6 and Nylon 6 Electrospinning

1.3.1 Brief Introduction to Nylon Polymer

The Dupont company start their development project in 1930 and in 1935, the first sample of Nylon was created out of diamines by Wallace Hume Carothers at DuPont's research facility[30]. Since then, Nylon becomes the first synthetic polymer fibers that undergoing mass production and the most successful commercial polymer[30].

The Nylon polymer has a linear polymer chain whose structural units are linked by amide groups. As a result, Nylon polymer's scientific name is polyamide. Generally there are two categories of polyamides. The first one is synthesized from diacids and diamines. This type of polyamide is identified as Nylon A,B in which A stands for the number of carbon atoms in diamine and B stands for the number of carbon atoms in the diacids. Nylon 6,6 is the one that of major commercial importance and the one that was fabricated in 1935[31]. The second one is sythesized from amino acids. They are identified as Nylon A, in which A stands for the number of carbon atoms in the monomer[31]. Nylon 6 is the most commercially important type in this category and it is used in this project. The structure of Nylon 6 is shown in Figure 1.8.

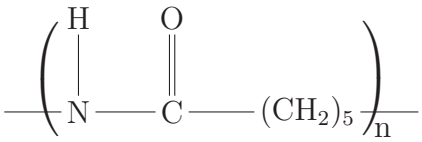

Figure 1.8: Structure of Nylon 6

1.3.2 Nylon 6 Electrospinning

Nylon 6 has a strong chemical resistance and it is inert in most of the organic solvents[31]. However, it has been discovered that formic acid and acetic acid is able to dissolve Nylon 6 at room temperature[32]. Also, acetic acid and formic acid are both volatile solvents, thus they make Nylon 6 ideal candidate for electrospinning[33]. Since at room temperature, the vapor pressure of formic acid (5.3kPa) is higher than acetic acid (1.5kPa), formic acid is the most frequently used solvent for Nylon 6 electrospinning in the literature[11, 15, 33–39].

Electrospinning of Nylon 6 polymer has been widely studied in the literature and the electrospun pristine Nylon 6 and Nylon 6 nanocomposites have a variety of applications. Quan Shi et al.[39], Kuitian Tan et al.[40] and Hem Raj Pant et al.[41] was electrospun Nylon 6 with various of additives including silver nanoparticles, gelatin and N-halamine additives. Good cell compatibility and antibacterial properties were demonstrated by them, which makes electrospun Nylon 6 nanofiber mats a potential candidate for biomedical engineering. In fact, electrospun Nylon 6 nanofiber mats have already been used as scaffold in tissue engineering by Abdalla Abdal-hay et al.[42, 43]. Another field that electrospun Nylon 6 nanofiber mats are frequently used is filtration and purification. Haitao Zhang et al.[44] were able to successfully electrospin hybrid Nylon 6/chitosan nanofibrous mats with diameter ranging from 80-310nm. They also showed that this nanocomposites is a potential candidate for the industrial purification of papain. Seongpil An et al.[45] decorated Nylon 6 nanofibers with titania nanoparticles for water purification while Mozhdeh Ghani et al.[46] fabricated Nylon 6/chitosan fibrous nanocomposties and used them for anioni dye removal.

In conclusion, the electrospinning of Nylon 6 is widely studied and the it has been used in various of applications.

1.3.3 Wettability of Nylon 6 polymer nanofibers

As for the applications mentioned in section 1.3.2, wettability is one of the most important properties and tunable wettability of Nylon 6 and Nylon 6-based nanocomposites is ideal in the practical applications. Although the electrospinning of Nylon 6 nanofibers and their applications are widely studied in the literatures, the number of literatures that mentioned the wettability of Nylon 6 is limited. Also, disagreements of the results exist in the literature.

Nylon 6 is considered hydrophilic since water is able to form hydrogen bonds with the

amide groups[31]. Affandi et al.[35] electrospun four different polymers including Nylon 6, polyvinyl alcohol (PVA), polyacrylonitrile (PAN) and copolymer polyvinylidenefluoride - hexafluoropropylene (PVDF-HFP) and characterized their wettability. In this work, Nylon 6 was categorized as a kind of hydrophilic polymer. The pure Nylon 6 casted film exhibited contact angle of 44±4° while electrospun Nylon 6 film with fiber diameter 109±16nm exhibited contact angle of 42±2°. The results they presented are reasonable since the contact angle of Nylon 6 bulk material is around 60° to 70°. Electrospun Nylon 6 nanofibers has a significantly increased surface-to-volume ratio and increased surface roughness. Hence, based Wenzel's model, the contact angle should be lower than the bulk material[27]. Dhineshbabu et al.[47] studied the wettability of cotton fabric and the non-woven electrospun Nylon 6 coated cotton fabric. They discovered that the cotton fabric is superhydrophilic but Nylon 6 coated cotton fabric is hydrophobic. It is possible since the substrate of the membrane may have a significant effect on the wettability of the membrane[24]. Abdalla Abdal-hay et al.[42, 43] found that pristine Nylon 6 nanofiber mats exhibited a contact angle of 132±3°. In fact, the contact angle data in this paper was acquired 1s after the deposition of the water drop. However, by the experimental results in this project, it is discovered that the water drop needs around 3 to 4s to relax to equilibrium state. Therefore, the contact angle data in this paper is not acceptable as the indication of the wettability. Hem Raj Pant and his group did several works on electrospun Nylon 6 and Nylon 6 nanocomposites and contact angle was one of their characterized properties[21, 41, 48–52]. However, the characterized contact angle data of pure Nylon 6 nanofibers ranges from 80° to 122°. In all, the wettability of Nylon 6 nanofiber mats and Nylon 6 fibrous nanocomposites was not widely studied and tunable wettability of that was never found in the literature.

1.4 Silica Nanoparticles

Silicon Dioxide (Silica) is one of the most commonly found inorganic substance in nature and it is widely used in personal care, food and pharmaceutical products[53]. Silica nanoparticles are widely used in filtration, biomedical sensing or drug delivery applications[54]. Due to its multifunctionality and good compatibility, silica nanoparticles have been embedded in a variety of electrospun polymers such as polymethyl-methacrylate (PMMA)[55], polyvinil alcohoa (PVA)[2], polyurethane (PU)[56] and polyvinylidene fluorid (PVDF)[57]. Silica nanopar-

ticles can also be used in the applications mentioned in section 1.3.2. Recently, Nylon 6/silica composites have also been successfully synthesized as the absorbent for solid phase micro-extraction[58]. Although silica nanoparticles are compatible with Nylon 6 and are also be able to disperse in formic acid, there is only limited literatures that studied the Nylon 6/silica fibrous nanocomposites. Islam et al.[33], Shi et al.[39] and Aghakhani et al.[59] all successfully electrospun Nylon 6 reinforced by silica nanoparticles. Both well distributed silica and agglomerated silica beads (see Figure 1.9) were reported in the literature. However, none of them discussed the effect of processing parameters on the end product. Therefore, silica nanoparticles are chosen as the reinforcement and fibrous Nylon 6/Silica nanocomposites is stuided in this project.

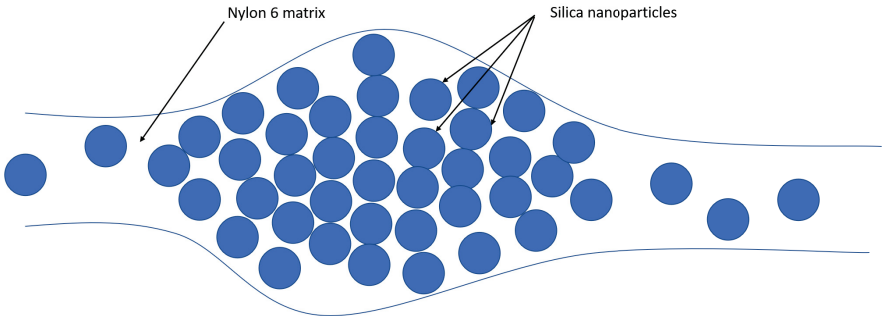

Figure 1.9: Agglomerated silica beads

1.5 Aim and Structure of the Thesis

The first aim of the study is to understand and optimize the effect of solution recipes on the fiber and bead morphology of electrospun silica reinforced Nylon 6 fibrous nanocomposites. The electrospun mats was characterized in both microscopic view and macroscopic view so that the effect of solution parameters on microscopic fiber properties and macroscopic mat surface properties can be discovered. All these works are presented in Chapter 2 and a design guidance of electrospun Nylon 6/silica fibrous nanocomposites is provided for the preparation of Chapter 3. After that, in Chapter 3, optimized solution recipes was used to fabricate electrospun Nylon 6/silica fibrous nanocomposites for tunable wettability study. Since Nylon 6 is a type of hydrophilic material, both equilibrium contact angle and imbibition process of the droplet was studied and the effect of Nylon 6 concentration and silica weight fraction was discussed. Finally, a conclusion and future work recommendation was provided in Chapter 4.

Chapter 2

Fabrication and Characterization of Electrospun Mats of Nylon 6/Silica Nanocomposites Fibers*

(*) A version of this chapter will be submitted to Journal of Engineered Fibers and Fabrics as a journal paper with authors: Yu Chen, Prashant Waghmare, Cagri Ayranci

2.1 Introduction

Due to the high surface-to-volume ratio and good physical properties of polymeric nanofibers, they are widely used in various applications, such as micro-filtration, protective clothing, optical sensor, *etc.*[2]. There are various techniques to produce polymeric fibers and nanofibers including solution spinning[1], drawing[3], self-assembly[4] and electrospinning[5]. Among them, electrospinning is regarded as the most versatile and tailorable technique because it offers the ability to produce ultrathin nanofibers with diameters ranging from tens of micrometers to several nanometers[10].

Polystyrene (PS)[60], poly(vinyl alcohol) (PVA) [61], polyvinylden fluoride (PVDF) [62], and polyamide 6 (PA6, a.k.a. Nylon 6 ®) [21, 41, 50, 51, 63] are some of the common examples of thermoplastic polymers used in electrospun fiber formation. Among these, Nylon 6 is an important polymer due to its biocompatible nature and good physical and mechanical properties. It is also one of the most commonly utilized polymers around the world. A number of researchers[21, 41, 50, 51, 63] have demonstrated the ability of forming Nylon 6 nanofibers in the range of 100nm to 300nm diameter and the electrospun Nylon 6 nanofiber mats are widely used in applications such as tissue engineering[64], wound-healing[20] and

filtration[65].

In electrospinning, fibers are often reinforced with nanoparticles to increase the mechanical properties or to tailor physical or chemical properties of the fibers and their mats. With the embedment of nanoparticles, the mechanical, physical and chemical properties can be enhanced and specific applications can be targeted[45, 66–68]. In many applications such as filtration and tissue engineering, tunable wettability is an ideal property. However, the wettability of Nylon 6 nanofiber mats is not widely studied in the literature with the exception of few publications. Affandi et al.[35] categorized electrospun Nylon 6 nanofiber mats as a hydrophilic material since it exhibited contact angle of 42±2°. However, Abdalla Abdal-hay et al.[42] found that Nylon 6 nanofiber mats is hydrophobic, as it shows a contact angle of 132±3°. The results are completely different in those two literatures.

Silicon dioxide (Silica) nanoparticles have been widely used in electrospun composite nanofibers due to its biocompatibility, filtration ability and tunable size[22, 36, 56, 69, 70]. Although Nylon 6/Silica composites have been successfully synthesized for the application of solid phase micro-extraction[58], there are only limited papers that studied the Nylon 6/Silica composites nanofibers. Md. Shahidul Islam et al.[33] fabricated Polyvinyl acetate coated Nylon 6/Silica nanocomposite membrane for oil-water separation but they did not discuss the effect of parameters on the morphology of the nanocomposites. Quan Shi et al.[71] fabricated Nylon 6/silica nanocomposites using 2,2,2-tri-fluoroethanol (TFE) as the solvent, however, the electrospinning parameters were not even presented. Ali Aghakhani et al.[59] synthesized silica nanoparticles by themselves and embedded the nanoparticles into Nylon 6 nanofibers. But the diameter of the synthesized silica nanoparticles is three times larger than that of the Nylon 6 nanofibers, so silica nanoparticles are not well distributed in the fibers and only bead-on-string morphology was created. None of them investigated the Nylon 6 concentration and silica weight fraction on the morphology of the nanocomposites.

Consequently, the present study investigates the fabrication and characterization of silica reinforced Nylon 6 nanocomposites. In particular, the effect of silica to Nylon 6 ratio (Silica weight fraction) is investigated to obtain smooth, non-beaded nanofibers. Morphology of the fibers and their mats were characterized macroscopically and microscopically. The work in this paper offers a guidance for fabrication of Nylon 6/Silica nanocomposites and it is a preparation of making fibrous nanocomposites with tunable wettability, which will be presented in another paper.

2.2 Methodology

2.2.1 Raw Material

Polyamide 6 was obtained from Sigma-Aldrich Canada Co., Oakville, ON (product #181110). The molecular weight of the Nylon 6 was 10,000 g/mol and the bulk density was 1.084g/ml. Formic acid with a purity of 88% was obtained from Fisher Scientific, Ottawa, ON (product #A118P-500). Silicon dioxide (Silica) nanoparticles were obtained from Sigma-Aldrich Canada Co., Oakville, ON (product #637238). The average density of silica nanoparticles was 2.4g/ml and the particles size ranges from 10nm to 20nm. All materials were used as obtained without further treatment.

2.2.2 Solution Preparation

Formic acid was added into the container with premeasured amount of Nylon 6 and silica nanoparticles. After that, the container was sealed with Teflon tape to avoid the evaporation of formic acid. The prepared solutions were stirred with a magnetic stir bar under room temperature for 24 hours until all the Nylon 6 pellets were dissolved. Finally, the solutions were sonicated for 1h to ensure full dispersion of silica nanoparticles. Solution with 4 levels of Silica weight fraction (including 0%) and 3 levels of Nylon 6 concentration were prepared in the present work as is shown in Table 2.1.

Table 2.1: Solution recipes and codings

Nylon 6 Concentration (wt%)	**Silica Weight Fraction (%)**			
	0	2	4	6
15	S0N15[1]	S2N15	S4N15	S6N15
17.5	S0N17.5	S2N17.5	S4N17.5	S6N17.5
20	S0N20	S2N20	S4N20	S6N20

2.2.3 Viscosity Measurement

The viscosity of the solutions was measured with Rheometer (Rheolab QC, Anton Paar) coupled to refrigerated/heating circulator (F12, Julabo GmbH). The measurement system was a double cylinder measuring cup (DG42, Anton Paar GmbH, Anton-Paar). Before the

[1]SX stands for X% of silica weight fraction in electrospun nanocomposite fibers. NXX stands for XX wt% of Nylon 6 in Nylon 6/formic acid solution.

measurement, the solutions were sonicated for 5min to ensure full dispersion. 20ml of the sample solution was poured into the measuring cup and the measuring system was sealed with parafilm to avoid the effect of formic acid evaporation. For each measurement, shear rate was set to increase gradually from $20s^{-1}$ to $100s^{-1}$ and the corresponding dynamic viscosity was plotted against shear rate.

2.2.4 Electrospinning Process

Before the electrospinning process, the solution was sonicated for another 5 mins to ensure full dispersion. Then the prepared solutions were filled into 10ml syringes with Eccentric Tips (305482, BD Canada, Mississauga, ON) and placed on a syringe pump (Legato 101, by GENEQ Inc., Montreal, QC). Needles (305178 BD Canada, Mississauga, ON) were blunted with a rotationary cutting tool and connected to the syringe. The collector of the electrospun nanofiber mats was a flat square metal plate with side length of 15cm covered with aluminum foil. The tip-to-collector distance was fixed at 10cm and the pumping rate was fixed at 2μl/min. The electrospinning voltage was controlled by a high voltage supply (model ES30P-5W/DDPM, by Gamma High Voltage Research, Inc., Ormond Beach, Florida, USA) and set to 24kV for all the electrospinning process. The positive electrode was clamped on the needle and the negative one was clamped on the collector. Each sample was electrospun for 30min to ensure that the thickness of the mat after peeling off from the aluminum foil would be in the range of 15 to 20μm. All the tests and characterizations were done at the central region of the collected area.

2.2.5 Scanning Electron Microscope (SEM) Characterization

The nanostructures of the fibrous nanocomposite mats were analyzed with a field emission scanning electron microscope (Zeiss Sigma FESEM featured with GEMINI column) with Energy Dispersion X-ray (EDX). All nanocomposite samples were coated with carbon with a thickness of 6nm by Leica ACE600 Carbon/Metal coater. EDX is used to proof the existence of silica nanoparticles.

For fiber diameter measurement, three samples for each concentration combination were made in random order. On each sample, five locations near the center of the collected area were chosen. The magnification rate was set to be 20,000. Fiber diameters were measured with ImageJ software and 100 measurements were randomly chosen for each sample, *i.e.*

each location will take 20 measurements. Statistical analysis of variance (ANOVA) was used to determine whether average fiber diameters and standard deviations of the fiber diameter measurements varied by different Nylon 6 concentrations, as well as the addition of silica nanoparticles. The null hypothesis was that there is no difference and the significance level α was set to be 0.01.

2.2.6 Porosity Measurement

The samples for porosity measurement were made for 1h to gain measurable thickness. The porosity of the mat was determined by Eqn. 2.1 [72].

$$\phi_{mat} = 1 - \frac{\rho_{mat}}{\rho_c} \tag{2.1}$$

where ϕ_{mat} is the porosity of the composite nanofiber mat; ρ_{mat} is the density of the composite nanofiber mat; and ρ_c is the density of the Nylon 6/Silica nanocomposite without voids. Small rectangular pieces of the samples with areas between 2500mm^2 to 4900mm^2 were cut from each sample and weighed by precision scale with precision of 0.0001g (Mettler Toledo AL-Model). The length and width of the sample were measured by a vernier caliper (Schut Digital Caliper, 0-300mm) and the thickness of the sample was measured by a micrometer (Schut CP01 Electronic Outside Micrometer, 0-25mm, 0.001mm). The density of the composite nanofiber mat ρ_{mat} was calculated by the above-mentioned measurements. The density ρ_c of the Nylon 6/Silica nanocomposite without voids is determined by Eqn. 2.2

$$\frac{1}{\rho_c} = \frac{1}{\rho_{N6}} W_{N6} + \frac{1}{\rho_{Si}} W_{Si} \tag{2.2}$$

where

ρ_{N6} = Nylon 6 density

ρ_{Si} = silica nanoparticle density

W_{N6} = weight fraction of Nylon 6

W_{Si} = weight fraction of silica

Therefore, with the help of Eqn. 2.2, the density of each silica weight fraction is calculated and listed in Table 2.2.

2.2.7 Surface Roughness Measurement

Surface roughness was measured by a profilometer (Zygo Optical Profilometer). Three replicates for each concentration combination were taken for surface roughness measurement

Table 2.2: density ρ_c of the Nylon 6/Silica nanocomposite without voids

Silica weight fraction (%)	0	2	4	6
Density (g/ml)	1.084	1.096	1.108	1.120

and on each replicate, five points were randomly picked and measured. The magnification rate for object lens was 50 and the magnification rate for eye lens was 2. The field of view was 0.72mm×0.54mm. The root mean square (RMS) of the assessed profile was used as the description of the measured surface roughness. The fifteen measurements of one recipe were averaged as the final value of the roughness.

2.3 Results and Discussion

2.3.1 Solution Characterization

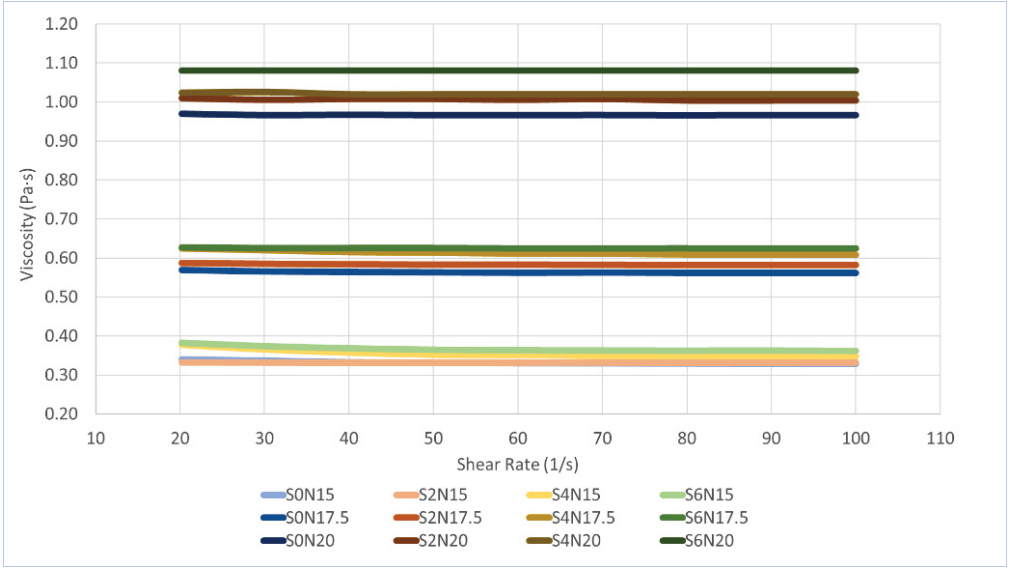

Figure 2.1: Viscosity measurement of the solutions

Viscosity is one of the key parameters that needs to be controlled for successful electrospinning. If the viscosity is too high or too low, the fibers will have defects, or the electrospinning process will not occur [51]. Figure 2.1 shows the viscosity versus shear rate data for Nylon 6 – Silica / Formic Acid solutions. In this figure, the legend SXNYY represents the solution with YYwt% of Nylon 6 concentration and X% of silica weight fraction, which is the same as the coding for the solutions in Methodology section of the manuscript. As

can be seen in Figure 2.1, the viscosity remains constant when shear rate increased gradually from $20s^{-1}$ to $100s^{-1}$. When Nylon 6 concentration is increasing, viscosity of the non-silica solutions rises steeply from $0.35Pa \cdot s$ to $1Pa \cdot s$. Comparing solutions with the same Nylon 6 concentration, the viscosity increases slightly by around $0.06Pa \cdot s$ when silica weight fraction increased from 0% to 6%. The reason accounting for this phenomenon is that viscosity is a measure of the internal resistance of a flowing liquid[61]. In the solutions studied here, the internal resistance is caused by the entanglement of Nylon 6 molecular chain and the inertia of the dispersed silica nanoparticles. Therefore, when Nylon 6 concentration is increased, there is more entanglement of Nylon 6 polymer chain, thus the viscosity is higher. Also, when the amount of silica is increased, their inertia provide a small amount of extra resistance, which results in the slight increase in the viscosity.

2.3.2 Microscopic Fiber Characterization

Pure Nylon 6 Nanofiber Characterization

In electrospun nanofibers, usually three types of morphologies can be achieved, namely bead, bead-on-string and smooth fibers[73]. Among these, super-thin, long and smooth nanofibers are preferred in most applications. On the LHS of Figure 2.2, the SEM images of fibers obtained with different Nylon 6 concentrations are shown. Smooth long super-thin nanofibers are randomly distributed on the collector to form a non-woven porous mat. The fiber diameter distribution of 300 measurements of each concentration are shown in the histogram on the RHS of each SEM image. It can be clearly seen in the histogram that the peak of the distribution shifts to the right when Nylon 6 concentration is higher. However, the shape of the distribution remains the same for all three levels of concentration. The averaged fiber diameter and standard deviation of the 300 measurements are shown in Table 2.3. When Nylon 6 concentration increased from 15wt% to 20wt%, the average fiber diameter increased from 103nm to 160nm while the standard deviation only increased from 11nm to 15nm. The increasing trend of average fiber diameter (with 95% confidence interval) by the Nylon 6 concentration can also be seen in Figure 2.3.

Single factor ANOVA analysis with $\alpha = 0.01$ was used to determine whether average fiber diameters varies by increasing Nylon 6 concentrations. The p-value of the test is less than 0.00001, which means that Nylon 6 concentration has a significant effect on average fiber diameter. The increasing trend of average fiber diameter results agrees with the viscosity

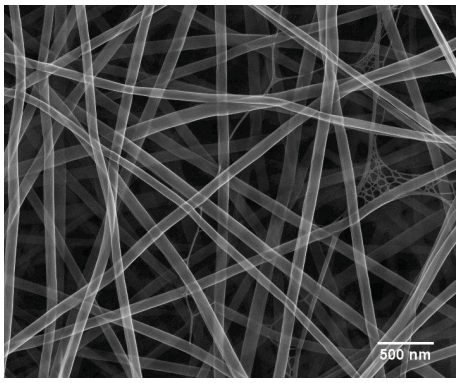

(a) S0N15 SEM

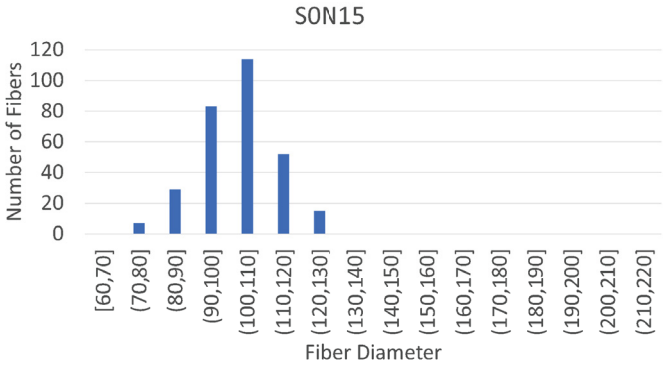

(b) S0N15 histogram

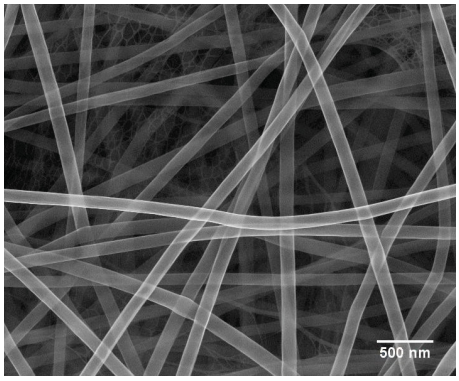

(c) S0N17.5 SEM

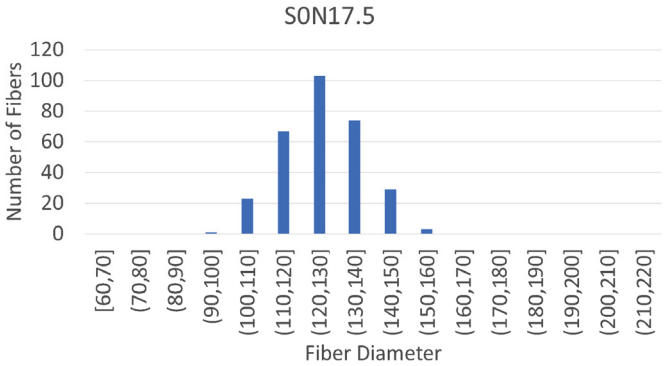

(d) S0N17.5 histogram

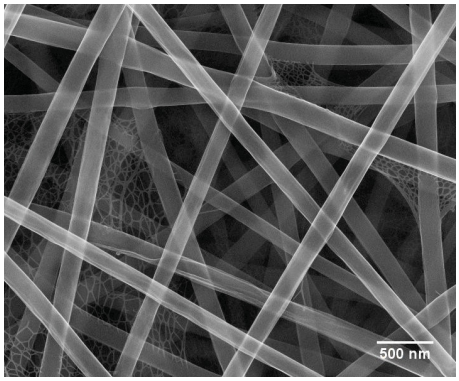

(e) S0N20 SEM

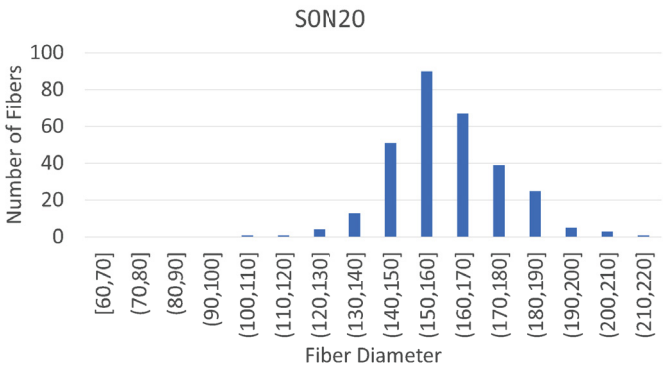

(f) S0N20 histogram

Figure 2.2: SEM images and histograms of pure Nylon 6 electrospun nanofibers

Table 2.3: average fiber diameter and standard deviation of the pure Nylon 6 nanofibers

Nylon 6 concentration (wt)%	**15**	**17.5**	**20**
Average Fiber Diameter±Standard Deviation (nm)	103±11	126±12	160±15

measurements presented above as higher viscosity will have more resistance on the elongation of the polymer material during electrospinning process[51].

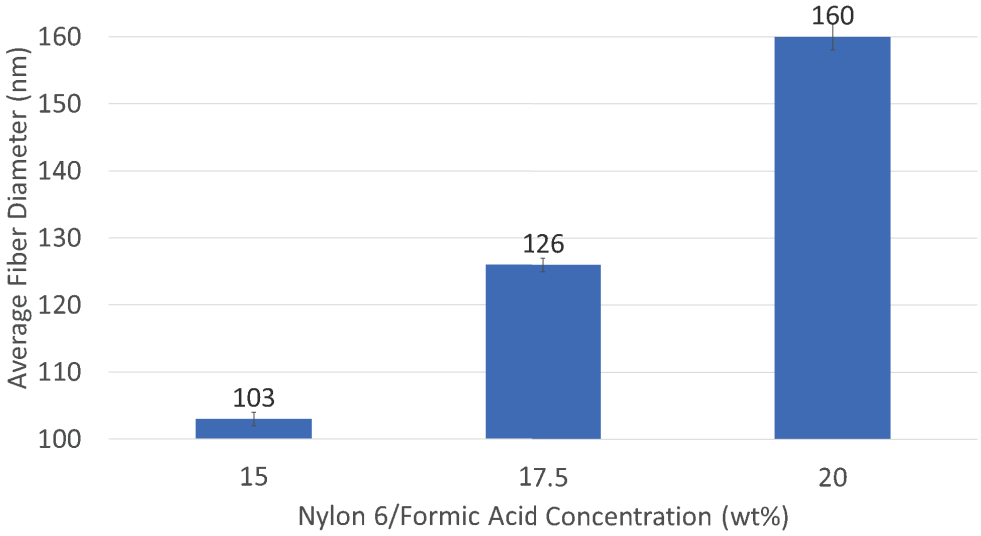

Figure 2.3: Average Fiber Diameter with 95% of confidence interval of Pure Nylon 6 Nanofibers

An interesting structure that exists in Figure 2.2 is the ultrathin spider-net like structure that are randomly distributed between the normal nanofibers. This is seen particularly for the bottom SEM image in Figure 2.2. The cause of this structure was investigated before [33] and it was concluded that under high voltage, the amide groups of Nylon 6 are partially ionized in some regions of the solution [33]. In those partially ionized and degraded regions, the entanglement of the polymer chains is reduced, thus the viscosity is reduced. During the electrospinning process, those low viscosity regions form a surface with solvent-rich parts and Nylon-rich parts thus phase separation occurs[63]. That is why in Figure 2.2, the spider-nets are covering and adhering to the fibers. Ding et al. [74] studied the bonding between spider-nets and nanofibers, they found that lower humidity can strengthen the bonding. In the present study, the relative humidity during electrospinning was very low (3%-5%). Therefore the results agrees with Ding's work [74]. Kuo et al. [65] claimed that the precursors of ultrathin spider-net structures were those ribbon-like fibers. They are stretched under large electrostatic forces and phase separation occurs before they hit the collector. However, among all the figures that presented in this paper, none of them can prove that those spider-nets were ribbon-like fibers during the start of the process. Kuo also mentioned that 60-days-old

solutions can have more spider-net structures during electrospinning process [65]. However, in the present study, all the electrospinning process were done within 7 days after the solution preparation. Therefore, no differences were found among the samples.

Nylon 6/Silica Nanocomposite Fibers

Figure 2.4, Figure 2.5, Figure 2.6 shows the fiber morphology and bead structure of fibers with 2%, 4% and 6% of silica nanoparticles respectively. Similar to Figure 2.2, the solution codings are labeled below the SEM images and histograms, and the average fiber diameter and standard deviation are shown in table 2.4. As can be seen in the SEM images, when silica weight fraction is increased up to 6%, smooth long super-thin nanofibers are still randomly distributed to form nonwoven mats.

Table 2.4: average fiber diameter and standard deviation of the Nylon 6/silica nanocomposite fibers (unit:nm)

Nylon 6 Concentration (wt%)	**Silica Weight Fraction (%)**		
	2	4	6
15	105±11	104±12	109±9
17.5	128±14	128±15	131±15
20	160±16	161±17	164±15

However, under the limited imaging resolution, it is difficult to determine whether the nanoparticles are imbedded on the fiber surface or within the fibers. EDX point analysis was used to prove the existence of silica nanoparticles along the fibers, as is shown in Figure 2.7b, 2.7d, 2.7e. The yellow solid spectrums are the spectrums taken from pure Nylon 6 nanofiber, which are used as references. As can be seen in Figure 2.7, the silicon(Si) peak exists in all the nonzero silica weight fraction samples, which means that the silica nanoparticles are distributed in the nanofibers.

The histograms of fiber diameter distribution are also shown on the RHS of SEM images in Figure 2.4, Figure 2.5 and Figure 2.6. Similar to the histograms shown in Figure 2.2, the peaks also shift to the right with the rise of Nylon 6 concentration. However, when comparing the histograms with samples from the same Nylon 6 concentration, they do not have any visible difference. Single factor ANOVA analysis with $\alpha = 0.01$ is also used to determine whether the increasing silica weight fraction would affect the average fiber diameter the Nylon 6/Silica nanocomposite fibers. The p-value of increasing silica weight fraction on average

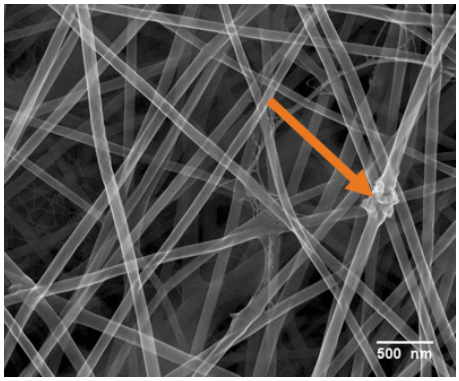

(a) S2N15 SEM

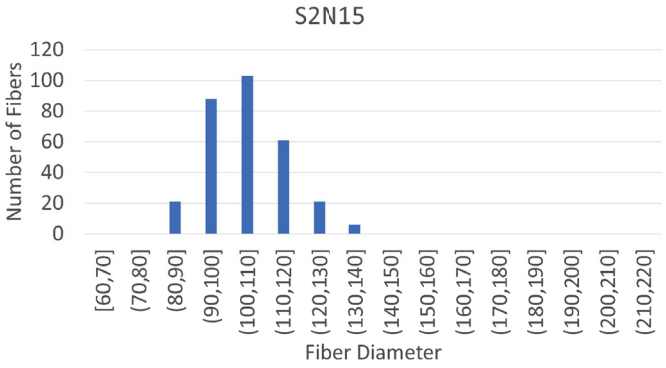

(b) S2N15 histogram

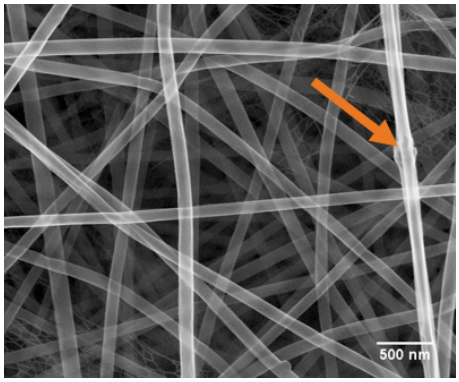

(c) S2N17.5 SEM

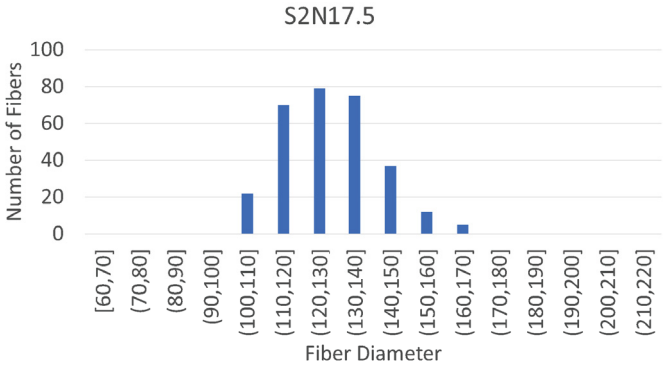

(d) S2N17.5 histogram

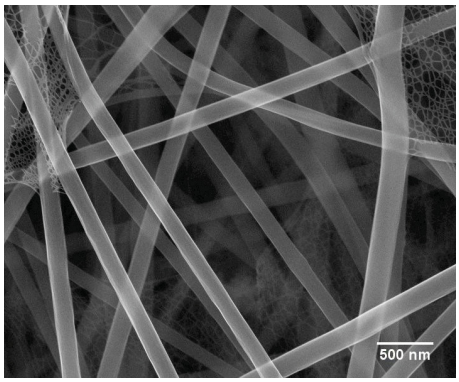

(e) S2N20 SEM

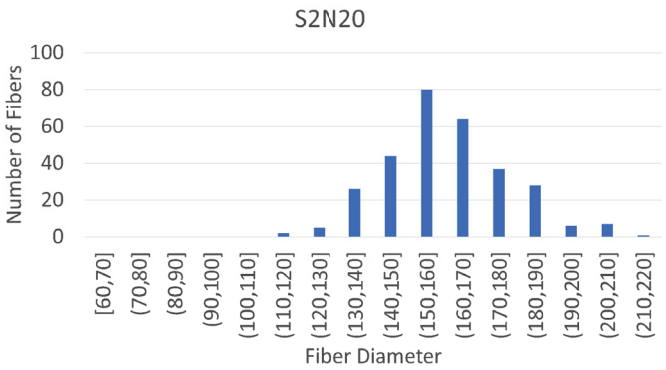

(f) S2N20 histogram

Figure 2.4: SEM images and histograms of Nylon 6 electrospun nanofibers reinforced with 2% of silica nanoparticles

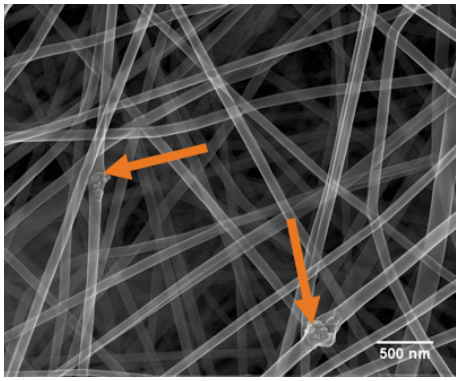

(a) S4N15 SEM

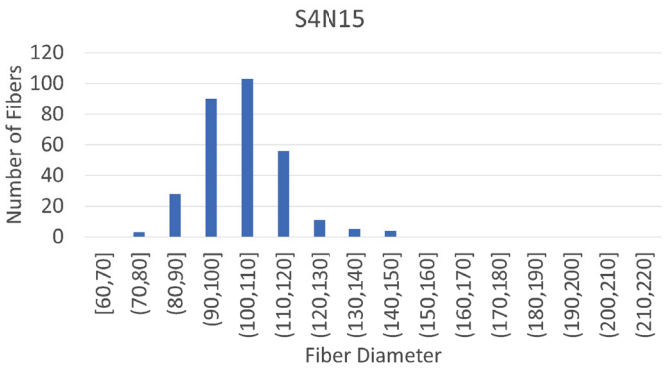

(b) S4N15 histogram

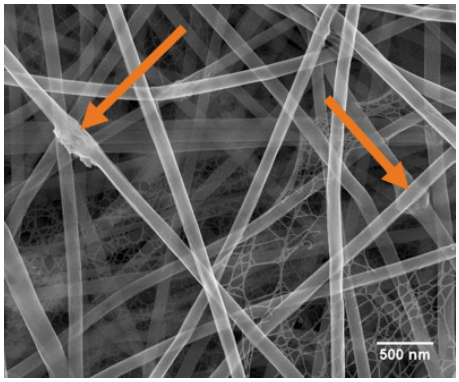

(c) S4N17.5 SEM

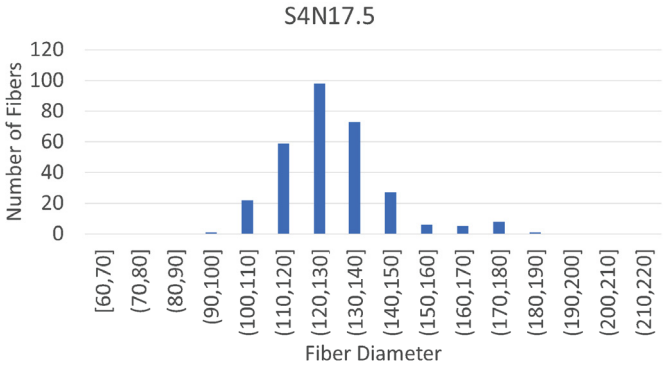

(d) S4N17.5 histogram

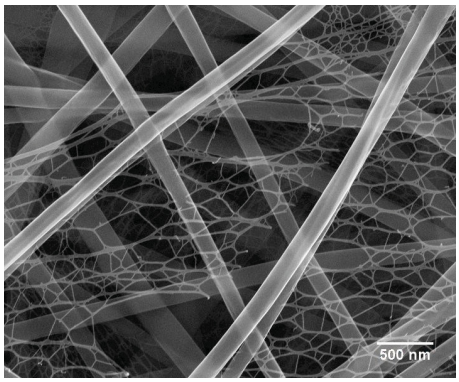

(e) S4N20 SEM

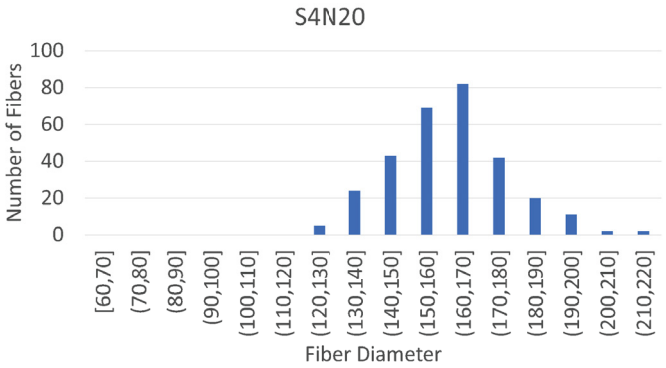

(f) S4N20 histogram

Figure 2.5: SEM images and histograms of Nylon 6 electrospun nanofibers reinforced with 4% of silica nanoparticles

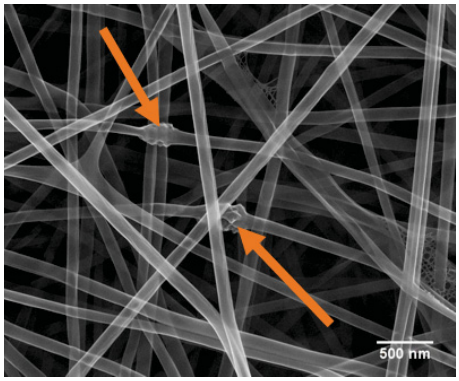

(a) S6N15 SEM

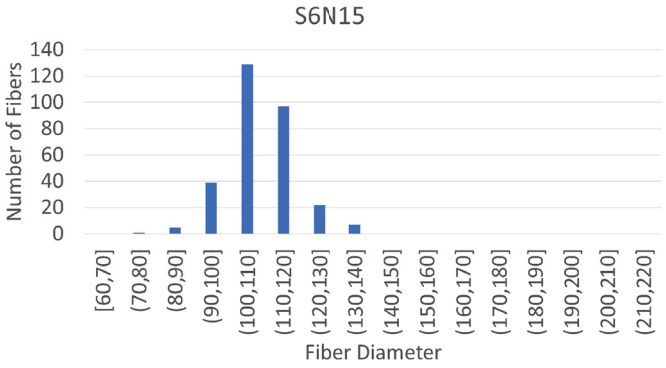

(b) S6N15 histogram

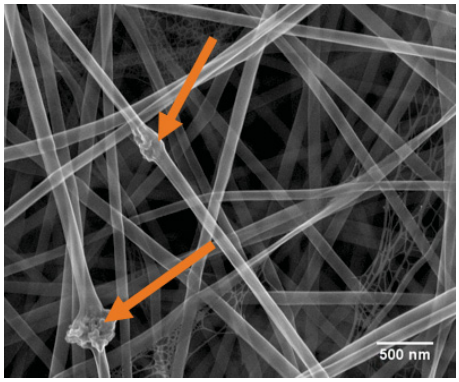

(c) S6N17.5 SEM

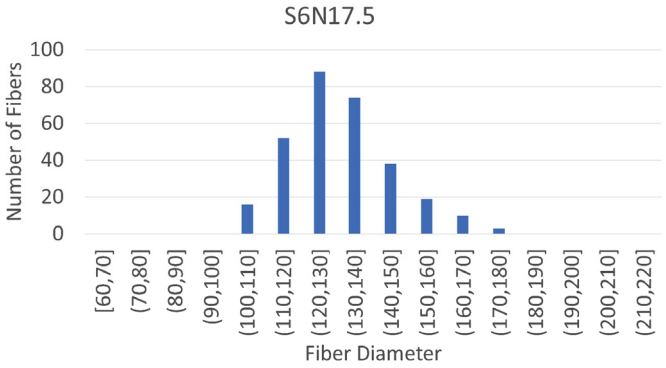

(d) S6N17.5 histogram

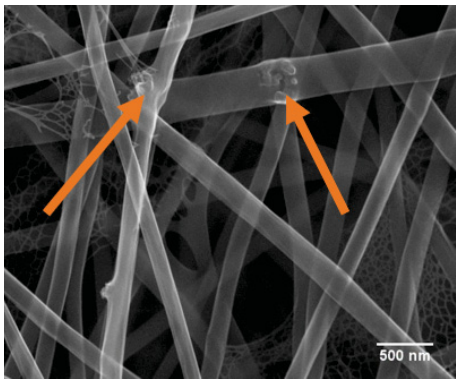

(e) S6N20 SEM

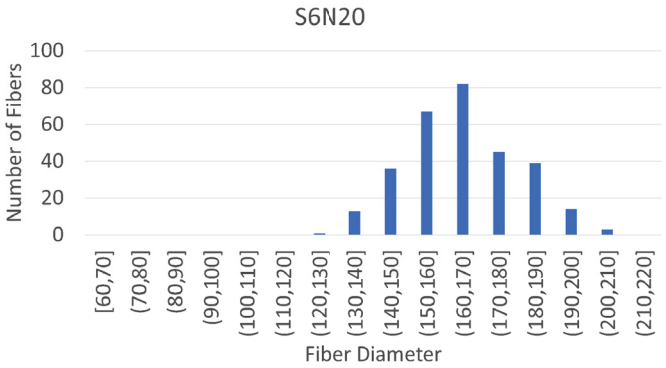

(f) S6N20 histogram

Figure 2.6: SEM images and histograms of Nylon 6 electrospun nanofibers reinforced with 6% of silica nanoparticles

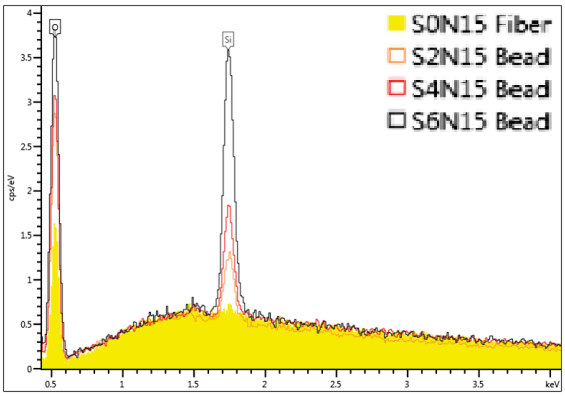

(a) 15wt% Nylon 6 Bead Comparison

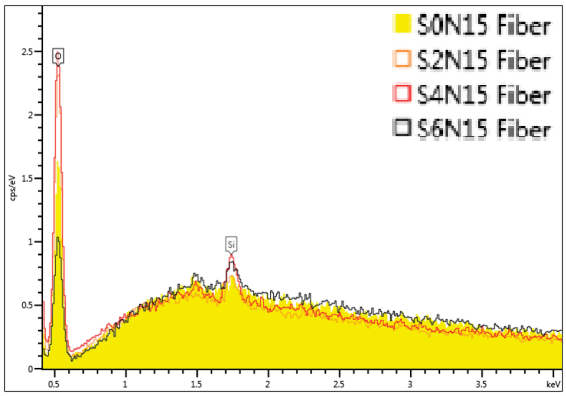

(b) 15wt% Nylon 6 Fiber Comparison

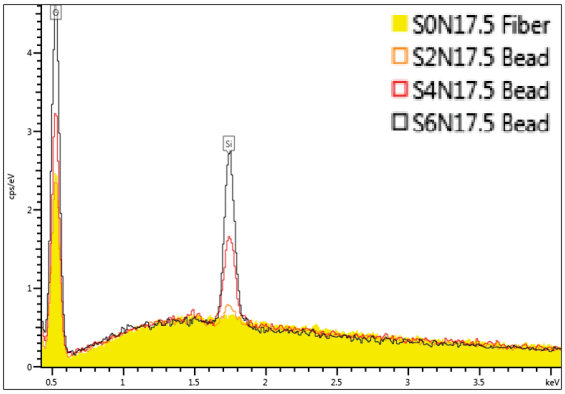

(c) 17.5wt% Nylon 6 Bead Comparison

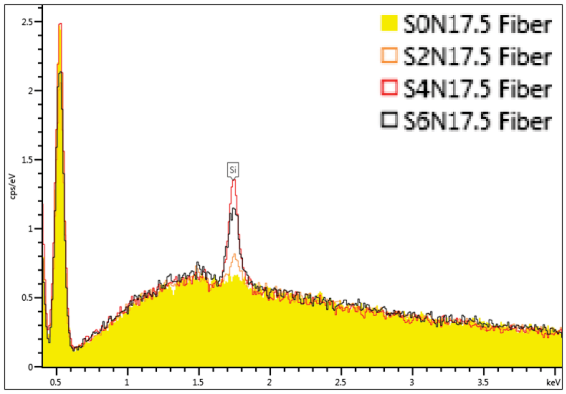

(d) 17.5wt% Nylon 6 Fiber Comparison

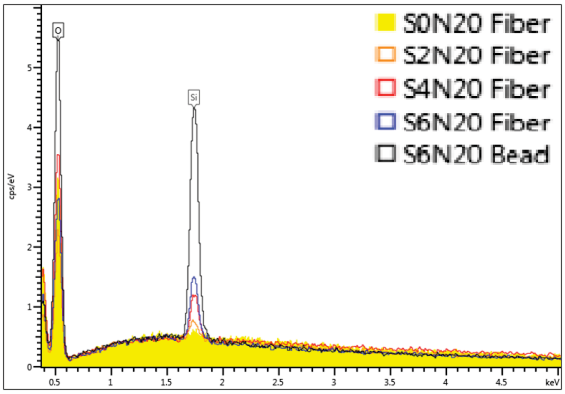

(e) 20wt% Comparison

Figure 2.7: EDX point analysis spectrum of the mats electrospun by different Nylon 6/Formic Acid concentration

fiber diameter is 0.000014, 0.04078 and 0.12447 for 15wt%, 17.5wt% and 20wt% of Nylon 6 concentration respectively. It means that for 17.5wt% and 20wt% of Nylon 6 concentrations, the increasing silica weight fraction up to 6% does not have a significant effect on the fiber diameter. But for 15wt% Nylon 6 concentration, the same proportion of silica nanoparticles has a statistically significant effect. More specifically, the average fiber diameter remains unchanged at 2% and 4% silica weight fraction but increases to 109nm when 6% of silica is added. A possible explanation is that there might be a critical value of silica weight fraction for each Nylon 6 concentration. When silica weight fraction is less than this critical value, the entanglement of the Nylon 6 polymer chain is not affected by the silica dispersion and the increasing of viscosity is only due to the inertias of the silica nanoparticles. When the silica weight fraction exceeds the critical values, the silica nanoparticle dispersion starts to affect the entanglement of the polymer chain, thus the fiber diameter is increased. Another quick test was done using S20N20 solution, which means that 20% of silica nanoparticles were added into the solution of 20wt% Nylon 6/Formic Acid. It was found that the average fiber diameter increased to 187nm as expected. Unfortunately, in S20N20, the fiber surface becomes rough and the aggregations of silica nanoparticles is severe. The internal mechanism of this critical value is worth to be studied in the future. Summarized fiber diameter with 95% confidence interval are shown in Figure 2.8.

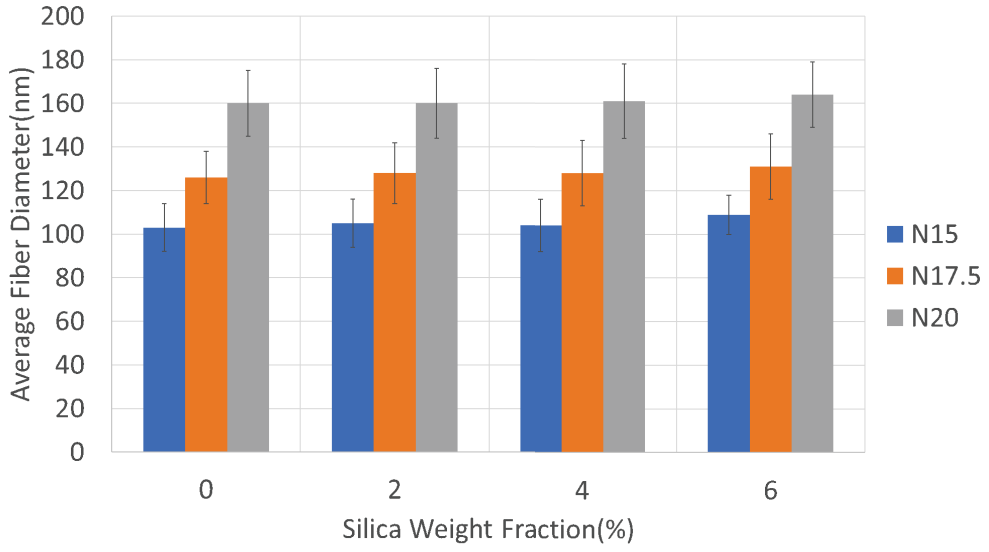

Figure 2.8: Average Fiber Diameter with 95% of confidence interval of Nylon 6/silica composite nanofibers

Similar to the non-reinforced case, spider-net structures can also be observed when silica nanoparticles are added (Figure 2.4, Figure 2.5 and Figure 2.6). The size, density, morphology and covering area of the spider-net structures are still random with no relationship to the silica addition. As is illustrated before, the spider-net structure is due to the ionization and degradation of Nylon 6 polymer chain. The silica nanoparticles are insoluble in formic acid and they are also nonconductive. Hence, the ionization of Nylon 6 has not been influenced during the electrospinning process.

Another interesting phenomenon is the formation of the agglomerated silica groups when silica nanoparticles are added. As is indicated by the arrows in Figure 2.4, Figure 2.5 and Figure 2.6, the silica beads were formed randomly in the entire nanocomposite mats. They are penetrated by the nanofibers, but the fiber diameter and morphology were not affected. The size and density of the beads have an upward trend with the increasing silica weight fraction. In 15wt% and 17.5wt% Nylon 6 concentration, small beads start to occur when silica weight fraction was only 2%, as is shown in Figure 2.4.

EDX point analysis was also done on those beads, as is illustrated in Figure 2.7a and Figure 2.7c in which the solid yellow spectrums are still pure Nylon 6 nanofibers. From the figures, silicon(Si) peak height rises steeply with the increasing silica weight fraction. For the samples with 20wt% Nylon 6 concentration, no significant difference was discovered when silica weight fraction increased up to 4% and only some small beads appears on the fibers with 6% silica weight fraction, as is shown by the arrows in Figure 2.6e. With the help of EDX point analysis in Figure 2.7e and EDX map analysis in Figure 2.9, it can be proved that the silica nanoparticles were distributed in the fibers but did not form beads in fibrous mats made by 20wt% Nylon 6 concentration.

From the above-mentioned results, it can be concluded that fibers made from lower Nylon 6 concentration are easy to be changed by silica addition. When Nylon 6 concentration is 15wt%, 2% of silica is enough to create beads. But when Nylon 6 concentration is increased to 20wt%, only small beads were occurred until 6% of silica nanoparticles are added. Also, for 20wt% Nylon 6 concentration, the average fiber diameter and standard deviation was maintained until 4% silica is added. In other words, when silica nanoparticles are added into the solutions to produce Nylon 6/Silica nanocomposites, there is a critical capacity that the Nylon 6 nanofibers could accommodate them. The critical capacity value is positive corelated to the average fiber diameter of the nanofibers. When the amount of silica exceeds

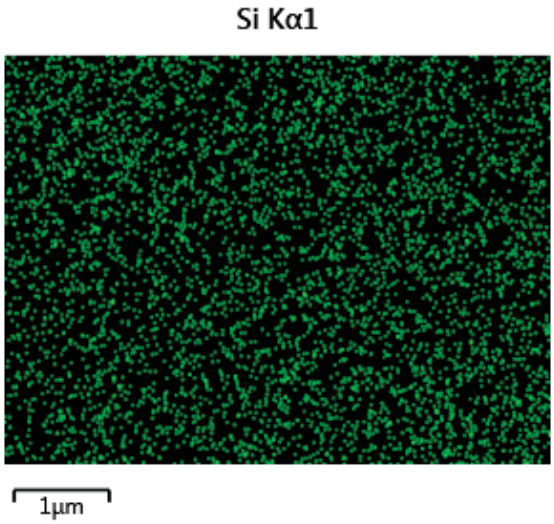

(a) S2N20

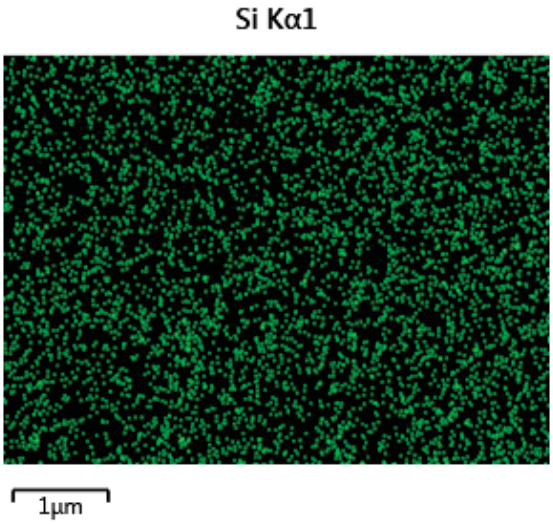

(b) S4N20

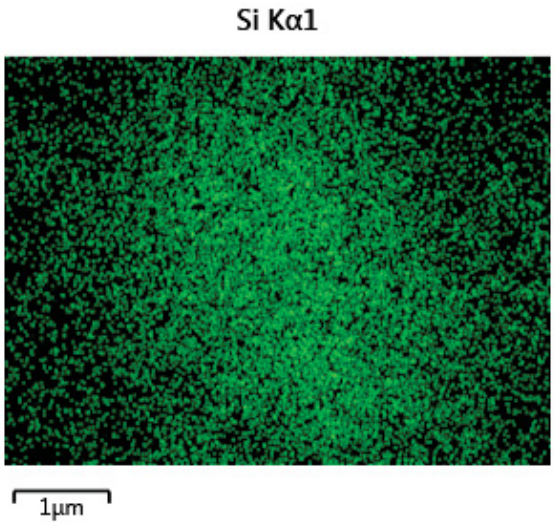

(c) S6N20

Figure 2.9: EDX map analysis spectrum of the mats electrospun by 20wt% Nylon 6/formic acid with different silica weight fraction

this critical value, beads start to occur. From the results in this paper, the critical value for 20wt% Nylon 6 concentration is more than 4% but less than 6%. For 15wt% and 17.5wt% Nylon 6 concentration, the critical value is less than 2% of silica weight fraction. Future work can be done to determine this critical value and investigate its internal mechanism.

2.3.3 Macroscopic Mats Characterization

Porosity

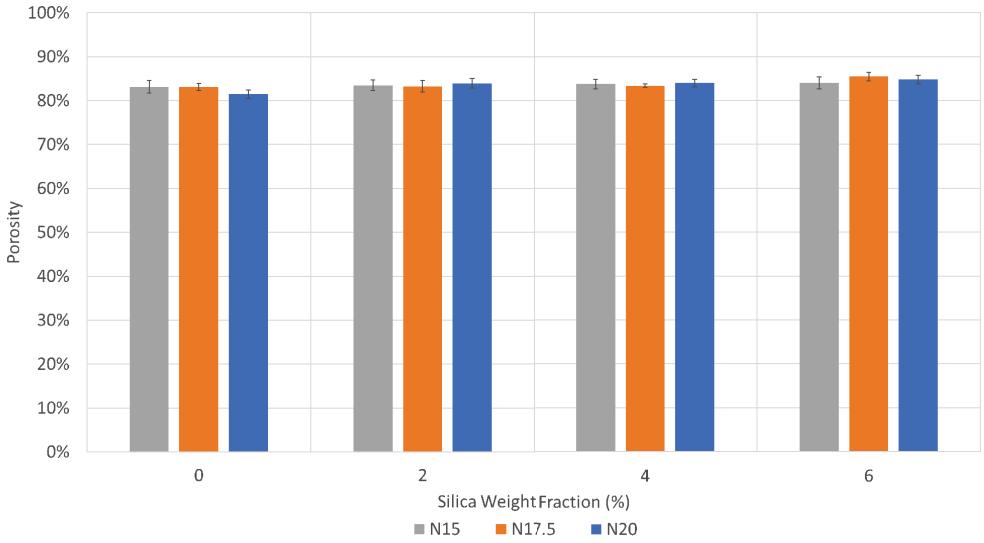

Figure 2.10: Porosity of the electrospun mats

Porosity is the measurement of proportion of voids in a certain material and it is one of the most important parameters for applications such as tissue engineering [64] and filtration[65]. As can be seen in Figure 2.10, the porosity of the electrospun mats remains at around 83% for all the solutions and the standard deviations of the porosity measurement are small and consistent. It means the electrospun mats are highly porous and the porosity value is not affected either by Nylon 6 concentration nor silica weight fraction. Although higher Nylon 6 concentration will deposit more mass of fibers on the collector, the volume of the mats is also increased due to the increasing spreading area. The reason for the rise of spreading area might be that solutions with higher Nylon 6 concentration have more charges so that the solution will experience more electric force in the electric field. As a result, the density of the mats is not affected, thus the porosity remains unchanged. As for the silica addition, Ding et al[36]. discovered that the addition of nanoparticles will create more nano-

cracks within the fibers. However, in this case, when silica weight fraction is lower than 6%, the volume of created cracks was too small comparing with the space between the nanofibers. Therefore, the porosity was also not affected by the silica addition.

Surface Roughness

Surface roughness is a quantification of the deviation of a real surface from an ideal flat surface. Other than material chemical structure, surface roughness is the most important parameter to determine the wettability of a material. As can be seen in Figure 2.11, surface roughness increases with the increasing of silica weight fraction regardless of the Nylon 6 concentration. The reason is that the addition of silica nanoparticles introduced more complexity and variation of the nanofibers such as beads.

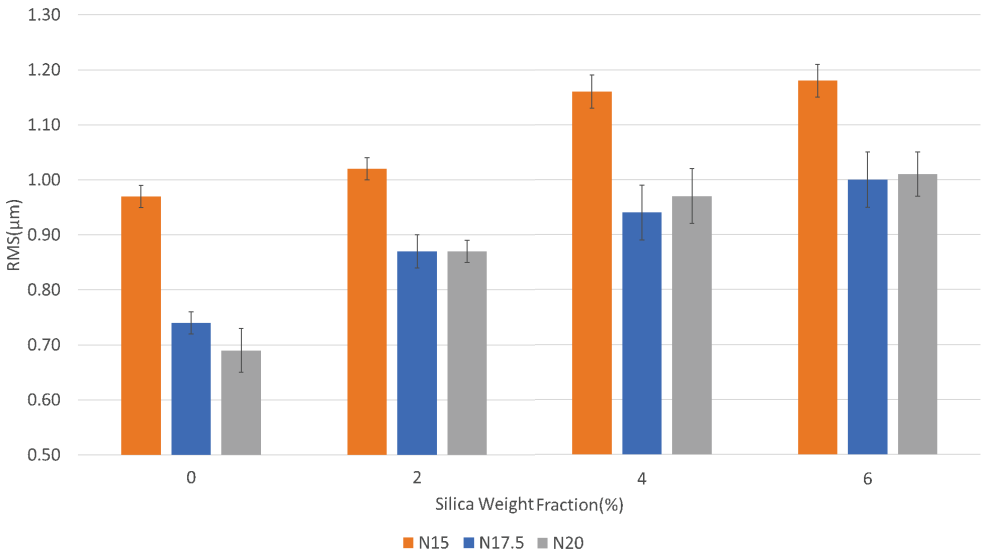

Figure 2.11: Surface roughness of electrospun mats

Another interesting phenomenon in Figure 2.11 is that the surface roughness of 17.5wt% and 20wt% Nylon 6 concentration is close but the surface roughness of 15wt% is significantly higher than both. There might be two reasons accounting for this phenomenon. First, lower Nylon 6 concentration gives thinner fibers. As is illustrated in Figure 2.12, when second layer of fibers were deposited on to the first layer, thinner fibers bend more thus the surface deviates more from the flat surface. However, this is not the main reason since the fiber diameter is in the range of 100-250nm. Hence, the change of surface roughness caused by the change of fiber diameter is limited. The second reason is that some portions with flat or

semi-flat fibers were discovered from time to time in the samples made from 15wt% of Nylon 6 concentration and these portions introduced heterogeneity of the surface. In these portions, there used to be smooth fibers but when unevaporated solvent was flying to them, the fibers were flattened by the solvent. This is considered as the main reason of the significantly high surface roughness of the mats made from 15wt% of Nylon 6 solutions.

(a) Fibers with higher fiber diameter

(b) Fibers with lower fiber diameter

Figure 2.12: Thinner fibers give higher surface roughness

2.4 Conclusion

In this paper, electrospun fibrous Nylon 6/silica nanocomposite mats were successfully fabricated. The microscopic and macroscopic characterization were done on the electrospun samples. It was discovered that when silica nanoparticles were not added into the solutions, all three Nylon 6 concentrations could produce smooth nanofibers and the fiber diameter increased from 103±11nm to 160±15nm. The effect of silica addition on the average fiber diameter of the mats was also investigated. For 17.5wt% and 20wt% of Nylon 6 concentrations, the average fiber diameter was not affected when silica nanoparticles were increased up to 6%. However, for 15wt% Nylon 6 concentration, the average fiber diameter remains unchanged when 2% and 4% of silica nanoparticles were added but it increased to 109±9nm when 6% of silica nanoparticles were added. Bead formation was also investigated in this paper. With the addition of silica nanoparticles, 15wt% and 17.5wt% started to form some aggregated silica beads at 2% silica weight fraction. However, 20wt% Nylon 6 concentration did not show any beads until 6% of silica nanoparticles was added. Surface roughness and porosity were also characterized and controlled. The surface roughness increased with the increase of silica weight fraction while decreased with the rise of Nylon 6 concentration. These two parameters were essential to the tunable wettability of electrospun fibrous Nylon 6/silica nanocomposites, which will be discussed in another paper.

Chapter 3

Tunable Wettability of Electrospun Fibrous Nylon 6/Silica Nanocomposites*

(*) A version of this chapter will be submitted to a journal as a journal paper with authors: Yu Chen, Cagri Ayranci, Prashant Waghmare.

3.1 Introduction

Electrospinning is an easy and versatile method to fabricate polymer fibers of different diameters ranging from several micrometers to tens of nanometers[10]. Electrospun Nylon 6/Silica fibrous nanocomposites is a promising candidate for applications such as microfiltration, tissue engineering and drug delivery[20, 33, 64, 75]. Nylon 6/Silica composites have also been successfully synthesized for the application of solid phase micro-extraction[58]. The surface property of these fibers is one of the decisive factors to dictate the applicability and the efficient outcome. Wetting on these fibrous materials by the liquid of interests is the indicator of the surface energy and surface properties. Here in this study, change in surface properties with respect to the morphological variation in the electrospun nanomaterials is investigated. Also, based on the surface characterizations such as wettability, imbibition process and surface roughness, a design matrix for the fabrication of desired electrospun mats is proposed.

Wettability is the description of surface energy of the substrate[23]. Apart from the polar and dispersed component of the liquid and solids, surface heterogeneity is another key aspect that decides the magnitude of liquid affinity or repellency towards the substrate[26]. Affandi

et al. [35] fabricated four different polymer nanofibers including Polyamide 6 (PA6 or Nylon 6), polyvinyl alcohol (PVA), polyacrylonitrile (PAN) and copolymer polyvinylidenefluoride-hexafluoropropylene (PVDF-HFP) and characterized their wettability. In their study, Nylon 6 nanofiber mats with fiber diameter 109±16nm was categorized as hydrophilic since it has a water contact angle of 42±2°. On the contrary, Abdal-hay et al. [42, 43] reported a water contact angle of 132±3° for the same material, indicating that Nylon 6 nanofiber mats are hydrophobic. Further, Pant et al.[21, 51, 63, 76] reported a wide range of contact angle from 80° to 122° for a variety of fibrous Nylon 6 mats. To the best of our knowledge, the detailed analysis for wettability of electrospun Nylon 6 with unified justification is missing in the literature. In this report, we have studied meticulously the wetting behavior of the pristine Nylon 6 and rationalized the observed wetting behavior based on several surface characterizations. In addition, the possibility of tuning the wettability by imbedding silica nanoparticles is also studied.

In the literatures, there are numerous ways to achieve tunable wettability of polymer nanofiber mats. But in most of the cases, the tuning is achieved either by modifying the surface structure of the individual fibers or controlling the diameter of the fibers. Kang et al.[77] used solvent chemistry to create small beads on the surface of the PS fibers. The existence of these small beads turned the hydrophobic PS membrane into superhydrophobic with a water contact angle of 154.2±0.7°. Generating bead structure along the fibers is another approach to change the surface roughness of the mats, by which can significantly alter the wettability. Zheng et al. [78] managed to fabricate PS membrane with various fiber structure including bead-only structure, bead-on-string structure and bead-free structures. The variation of the nanostructure changed the membrane wettability towards water. The contact angle of 158.1±2.4° was obtained when a thin layer of PS bead-free fibers was electrospun on the bead-only structure. In addition to the fiber surface structure, fiber diameter also plays an important role in tunable wettability of the membrane. Zhou et al. [79] found that by simply tuning the poly (vinylidene fluoride) (PVDF) concentration in the electrospinning solutions, different fiber diameters were achieved and the water contact angle increased with the rise of average fiber diameter.

Another major method is to reinforce the nanofibers with diverse nanoparticles. Recently, Dufficy et al. [80] imbedded hydrophobically- and hydrophilically-modified fumed silica nanoparticles into polyacrylonitrile (PAN) nanofibers by a one-step electrospinning

process. The apparent water contact angle was achieved from 28.1±2.3° to 133.3±8.3°, which suggests that electrospun PAN/Silica fibrous nanocomposite mats can be tuned from hydrophilic to hydrophobic. In similar way, Liu et al. [81] loaded ZnO nanoparticles into PVDF electrospun nanofiber mats and the contact angle in the range of 127° to 171° was achieved by altering the nanoparticle concentration.

Apart from these two major methods, the wettability can be tuned by other means such as electroactivation [60] or electrospinning the fibers on a functional substrate [82]. Ghochaghi et al. [60] fabricated nanofiber mats on a piezoelectric substrate. When an electric filed is applied, the substrate deformed, and the nanofibers were aligned and stretched. Thus, the surface roughness and porosity were changed. As a result, the average water contact angle decreased by 9.6±1.9° after the application of electric field. Kakunuri et al.[82] electrospun cellulose acetate nanofibers onto Nylon meshes with different pore size. The water contact angle was changed from 30.3±0.4° to 137.7±0.1°. These methods usually involve the special arrangements and it can be only considered for specific applications.

It is evident that the first two methods, namely control of fiber diameter and embedment of nanoparticles, are the appropriate ways that can provide the precise control for tunable wettability. In this study, Nylon 6/Silica nanocomposites were successfully fabricated, and the wettability of the mats with different fiber diameters and silica weight fractions is studied. The micro/nano-structure of the electrospun fibrous nanocomposite mats were also characterized and discussion on the effect of structure on the wettability is provided. Finally, a design guidance for the role of infusion of silica nanoparticles is also discussed.

3.2 Experimental Methodology

3.2.1 Raw Material

Polyamide 6 pellets (molecular weight 10,000 g/mol and the bulk density 1.084g/ml, product #181110) and Silicon Dioxide nanoparticles (particle size 10-20nm and average density 2.4g/ml, product #637238) were purchased from Sigma-Aldrich Canada Co., Oakville, ON. Formic acid with a purity of 88% (product #A118P-500) was supplied from Fisher Scientific, Ottawa, ON. All raw materials were used as supplied without purification or treatment.

3.2.2 Solution Preparation

Pre-measured amount of Nylon 6 pellets was added into the container along with specified amount of silica nanoparticles. After that, formic acid was added into the container and the container was sealed with Teflon tape to avoid the evaporation of formic acid. The prepared solutions were stirred under room temperature for 24 hours until all the Nylon 6 pellets were dissolved. Finally, the solutions were sonicated for 1h to ensure full dispersion of the silica nanoparticles. In the present work, 4 levels of Silica weight fraction (including 0%) and 3 levels of Nylon 6 concentration were prepared for electrospinning as is shown in Table 3.1.

Table 3.1: Solution recipes and codings

Nylon 6 Concentration (wt%)	**Silica Weight Fraction (%)**			
	0	3	6	9
17	S0N17[1]	S2N17	S4N17	S6N17
18.5	S0N18.5	S2N18.5	S4N18.5	S6N18.5
20	S0N20	S2N20	S4N20	S6N20

3.2.3 Electrospinning Process

Before the electrospinning process, the prepared solutions were sonicated for another 5min and filled into syringes (10ml, 305482, BD Canada, Mississauga, ON). G20 needles (305178 BD Canada, Mississauga, ON) were blunted with rotationary cutting tools and connected to the positive electrode of the high voltage supply. The syringes were placed on the syringe pump and the pumping rate was fixed at 2.5μl/min. A metal plate (side length of 15cm) covered with aluminum foil was used as a collector. It is placed 10cm away from the needle tip and connected to the negative electrode of the high voltage supply. The electrospinning voltage is controlled by a high voltage supply (model ES30P-5W/DDPM, by Gamma High Voltage Research, Inc., Ormond Beach, Florida, USA) and fixed 24kV was applied for all the electrospinning process. All samples were electrospun for 30min and instantaneously the deposited mat was peeled off from the collector for further characterization. All characterization processes were done at the central region of the collected samples. The details of the fabrication process and the parameters optimization guidance can be found elsewhere[15].

[1]*S# is % of silica weight fraction in electrospun nanocomposite fibers and N## is wt% of Nylon 6 in Nylon 6/formic acid solution.

3.2.4 Characterization Methods

Nanostructure analysis by Scanning Electron Microscope (SEM)

A field emission scanning electron microscope (Sigma FESEM featured with GEMINI column, Zeiss, Germany) was used to analyze the nanostructure of the samples, including fiber morphology, fiber diameter and silica embedment morphology. Before the SEM characterization, 6nm of carbon nanoparticles were deposited using a sputter coater (Leica ACE600 Carbon/Metal coater, Leica Microsystems, Canada). Two samples of each kind were fabricated for SEM characterization and five random locations were selected on the samples. Attempts were made to image the samples that was close to the center region of collector. The magnification of the SEM was maintained at the same level for all the characterization. For fiber diameter measurements, 20 readings were taken from each SEM image, *i.e.*, 200 measurements for each type of sample.

Surface Roughness Measurement by Optical Profilometer

An optical profilometer (Zygo Optical Profilometer, Zygo Corporation, Connecticut, USA) is used to measure the root mean square (RMS) of the assessed surface. The selected magnification for object-lens was 50 and eye-lens was 2. The field of view was 0.72mm×0.54mm. For each type of sample, two mats were fabricated separately, and five points were randomly picked for surface roughness characterization. As is mentioned earlier, the surface roughness of the samples was measured at the center of collector region. Minimum ten measurements were used for statistical analysis.

Porosity Measurement

The porosity of the mats is determined by comparing the measured density of the actual mats with the density of the void-free composites. The density of void-free Nylon 6/Silica nanocomposite ρ_c, is calculated by Eqn. 3.1 [83] where the density is considered in g/ml.

$$\frac{1}{\rho_c} = \frac{1}{\rho_{N6}} W_{N6} + \frac{1}{\rho_{Si}} W_{Si} \tag{3.1}$$

Here

ρ_{N6} = Nylon 6 density

ρ_{Si} = silica nanoparticle density

W_{N6} = weight fraction of Nylon 6

W_{Si} = weight fraction of silica

The calculated density of the void-free composites for each solution recipe is reported in Table 3.2 The density of the composite nanofiber mat ρ_{mat} was determined by measuring

Table 3.2: density ρ_c of the Nylon 6/Silica nanocomposite without voids

Silica weight fraction (%)	0	3	6	9
Density (g/ml)	1.084	1.102	1.120	1.140

the mass and the volume of the electrospun mats. The samples for porosity measurement were electrospun for one hour to ensure enough thickness to peel off and measure. Small rectangular pieces with length and width between 30mm to 70mm were cut from the sample then peeled off with extreme cautious to ensure no material was left on the aluminum foil. The mass of the sample was measured by a precision scale with precision of 0.0001g (Mettler Toledo AL-Model, Mettler-Toledo, LLC, Columbus, USA). A vernier caliper (Schut Digital Caliper, 0-300mm, Schut Geometrishce Messtechnik GmbH, Trossingen, Germany) was used to measure the length and width while a micrometer (Schut CP01 Electronic Outside Micrometer, 0-25mm, 0.001mm, Geometrishce Messtechnik GmbH, Trossingen, Germany) was used to measure the thickness of the mats.

Based on the information of the density, the porosity of the samples ϕ_{mat} was determined as [72].

$$\phi_{mat} = 1 - \frac{\rho_{mat}}{\rho_c} \tag{3.2}$$

Water Contact Angle Measurement by DSA 100E

The water contact angle was measured by a goniometer (DSA 100E, KRÜSS GmbH - Germany). After peeling off from the aluminum foil, the samples were gently clamped on a circular sample holder with a defined and uniform circumferential tension[24]. Five distilled water droplets (1μl) were deposited on different locations to obtain the wetting characteristics. The behavior of the droplets was recorded for up to 3 minutes until the drop was completed absorbed. All the measurements were performed at the room temperature with the relative humidity around 20%. The majority of the samples are hydrophilic in nature with porosity higher than conventionally reported fabric in the literature[31]. Obtaining an equilibrium static contact angle is always challenging task for such a porous hydrophilic

material [24]. Based on the transient variation in the drop radius and contact angle one can determine the appropriate way to determine the equilibrium contact angle [24]. The reported equilibrium contact angles are measured at the instant when drop attains the equilibrium without changing the base diameter.

3.3 Results and Discussion

3.3.1 Fiber Morphology and Bead Structure of the Electropsun Nanofiber Mats

The micro-structure of the electrospun mats are shown in Figure 3.1. As can be seen in Figure 3.1, the non-silica solutions all produce smooth nanofibers with spider-net-like structure that appear from time to time. The fiber diameter increased steeply with the increase of Nylon 6 concentration and raised slightly with the addition of silica weight fraction. The standard deviation in the fiber diameter measurement is less than $\pm$20nm, which suggests that the nanofibers are uniformly distributed. Spindle-like silica beads appeared in the images when silica weight fraction gradually increased from 0% to 9%. However, the silica weight fraction at which the silica beads start to form is different for different Nylon 6 concentration. For electrospun mats made from 17wt% Nylon 6 solutions, beads started to form at the surface of fibers when 3% of silica nanoparticles were added. In case of 18.5wt% and 20wt% of Nylon 6, spindle-like beads were formed when 6% and 9% of silica nanoparticles were reinforced. In lower silica weight fractions without beads formation (S3N18.5 and S6N20), small beads on the surface of the fibers were observed, and for S3N20, all silica nanoparticles were contained within the fibers. The existence of silica nanoparticles in the fibers and beads was inspected by the EDX characterization. When silica nanoparticles were added, the EDX spectrum confirmed the presence of silica with the appearance of silicon peak and the corresponding peak height increased with the bead size. Details of variations in the bead configurations and changes in the fiber morphology is reported in Chapter 2.

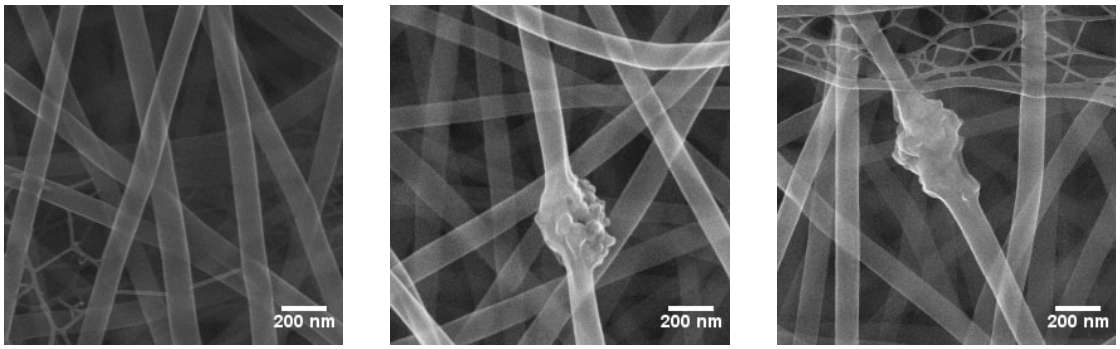

(a) S0N17 (114±9nm) (b) S3N17 (115±8nm) (c) S6N17 (117±9nm)

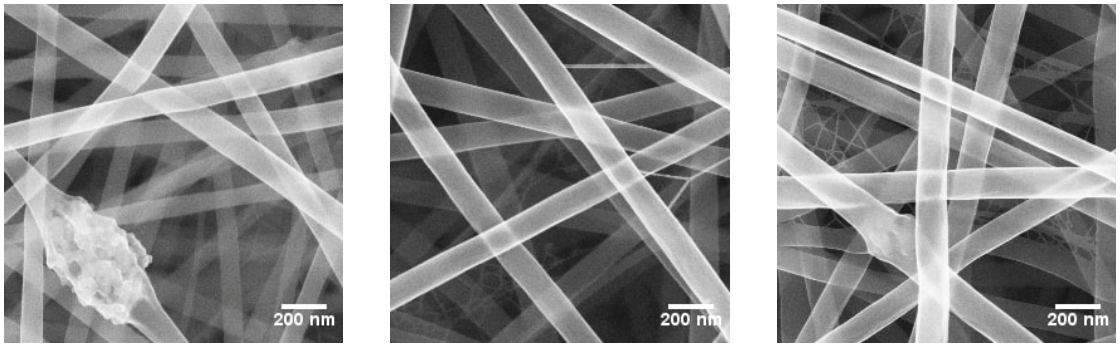

(d) S9N17 (121±11nm) (e) S0N18.5 (143±10nm) (f) S3N18.5 (144±13nm)

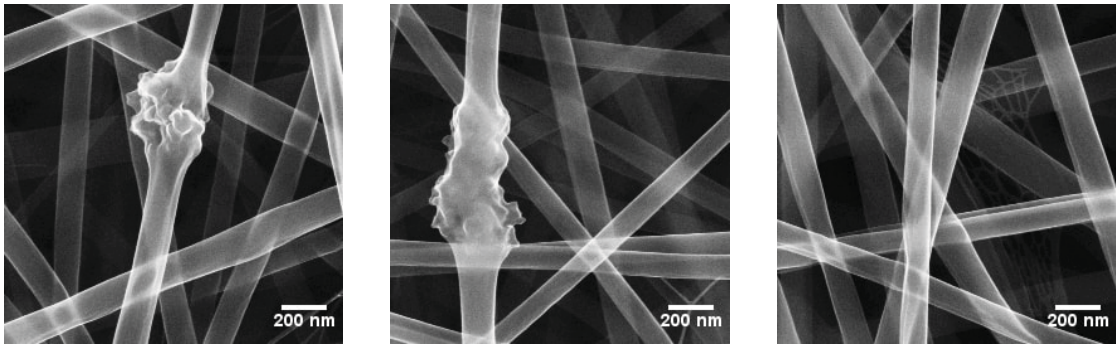

(g) S6N18.5 (147±18nm) (h) S9N18.5 (149±15nm) (i) S0N20 (157±13nm)

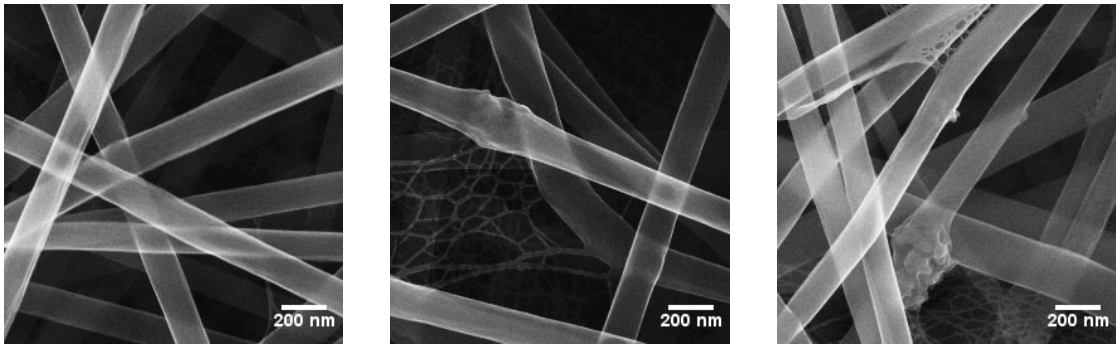

(j) S3N20 (160±15nm) (k) S6N20 (162±16nm) (l) S9N20 (166±20nm)

Figure 3.1: SEM images, average fiber diameter and standard deviation of the electrospun mats

3.3.2 Macroscopic Surface Properties of the Electropsun Mats

Surface Roughness

Surface roughness measurement results are shown in Figure 3.2. In the absence of silica nanoparticles, the surface roughness reduced with the increase of Nylon 6 concentration. This decrease in the surface roughness can be attributed to the increment in the average fiber diameter, which agrees with the results from Choi's work [84] and Beigmoradi's work [85]. As is mentioned in Chapter 2, the aspect ratio of the fibers decreases with the increment in the fiber diameter. This can be one of the reasons for decrease in the surface roughness as fiber diameter was increased. As for the silica addition, the surface roughness value increased with the increase of silica weight fraction, which is similar to the results given by Azarian et al. [86]. In most cases when silica is added, small beads on the fibers and spindle-like silica beads started to form, which is shown in Figure 3.1. Those micro-/nano- structures created more heterogeneity on the surface structures. Therefore, the surface profiles deviate more from the ideal flat surface. Hence, the surface roughness was increased with the increase of silica weight fraction.

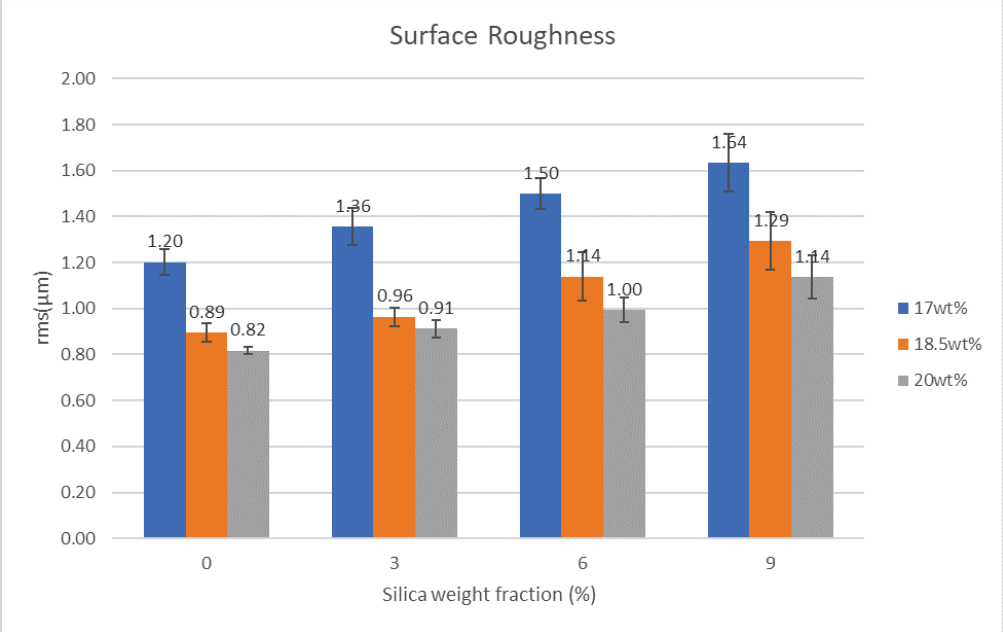

Figure 3.2: Surface roughness of the electrospun mats

Porosity

Among all the characterized properties, porosity is the only parameter that was not significantly affected. The porosity of the mats made by different Nylon 6 concentration and silica weight fraction are shown in Figure 3.3. We can see from the figure that, without silica reinforcement, the porosity for the mats with different Nylon 6 concentration was approximately 83% with similar standard deviation. These observations are in good agreement with the previously reported results in the literature [15]. When silica nanoparticles are added up to 9%, the porosity of all three Nylon 6 concentration was increased marginally by 4.44% to 6.38%. This small amount of increase was due to the embedment of silica nanoparticles inside the fibers [36]. In conclusion, the porosity was not significantly varied due to the change in the solution composition. As a result, we have not considered the role of porosity in the further analysis, in particularly for droplet spreading and wetting of the mats.

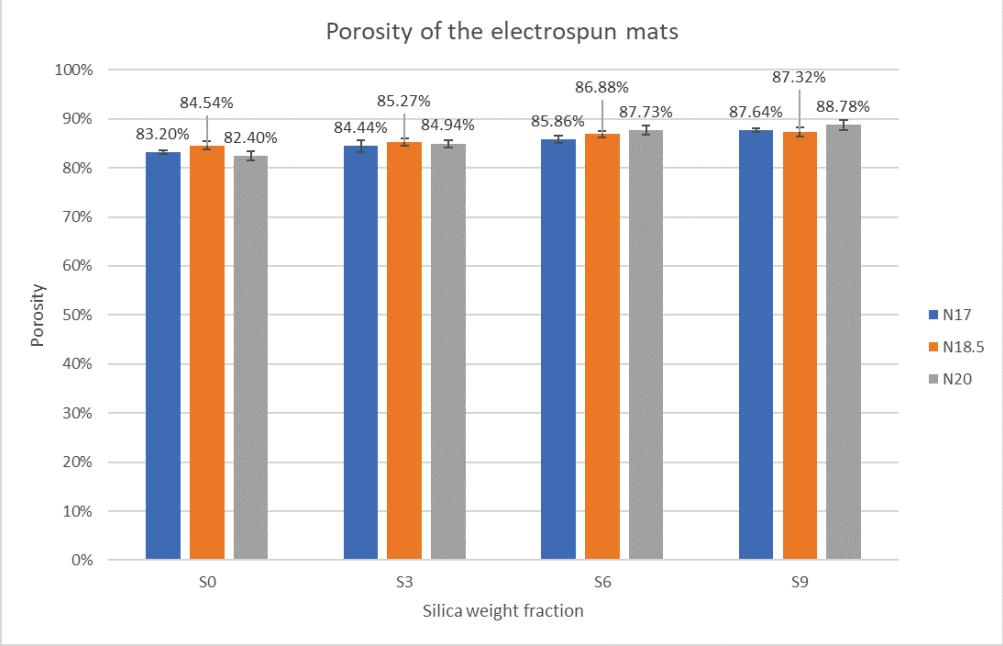

Figure 3.3: Porosity of the electrospun mats

3.3.3 Equilibrium Water Contact Angle

As is mentioned in the literature [77–81], both the surface energy of the nanoparticles and the change of micro-/nano- structure will change the wettability of the electrospun nanofiber mats. As can be seen in Figure 3.4, the equilibrium contact angle of pristine Nylon

6 nanofiber mats are less than 90°, which suggests the hydrophilic nature of the fibers. A similar observation was reported by Affandi et al. [35]. In this figure, Group S0, S3, S6 and S9 are representation of percentage of the silica nanoparticles reinforced in the nanofiber mats.

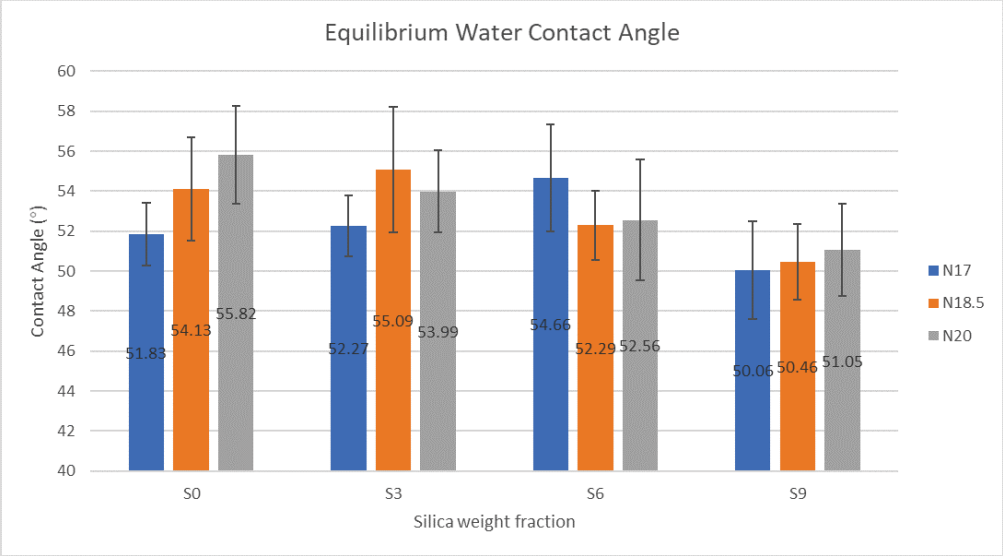

Figure 3.4: Equilibrium water contact angle of the electrospun mats

The equilibrium contact angle increased from 51.83±1.56° to 55.82±2.44° as Nylon 6 concentration increased from 17wt% to 20wt%. Based on Wenzel's wetting model, for hydrophilic materials, rougher surface will improve its hydrophilicity [27]. Referring to Figure 3.2, the surface roughness decreased with the rise of Nylon 6 concentration. Therefore, according to Wenzel condition argument, the contact angle should increase with the decrement in the roughness, which agrees with the experimental results stated above. However, the contact angle in Affandi's paper [35] was 42±2°, which is not in the contact angle range obtained in this study. In their study, the fiber diameter was 109±16nm, which is lower than S0N17(114±9nm). Therefore, if we follow the similar trend that we observed in the case of the surface roughness, the surface roughness for the mats with fibers thinner than S0N17 might have higher surface roughness, which results in even lower contact angle.

The effect of silica nanoparticles on equilibrium contact angle is more complicated than diameter of the fibers. As can be seen in Figure 3.4, for N17 electrospun mats, the equilibrium contact angle marginally increased from 51.83±1.56° to 54.66±2.66° for 0% to 6% silica weight fraction. Surprisingly, it decreased to 50.06±2.45° for 9% of silica weight fraction.

It is worthwhile to say that the effect of the silica particle does not affect the wettability significantly and it is confirmed after performing similar wettability studies for N18.5 and N20 samples. In the case of the N18.5, the peak of equilibrium contact angle of 55.09±3.14° was observed for S3N18.5 and the wettability was marginally reduced to 50.46±2.30° for S9N18.5. However, for N20 electrospun nanofiber mats, the equilibrium contact angle slightly decreased from 55.82±2.44° to 51.05±2.30° for 0% to 9% silica weight fraction. Based on the supplier's information (Sigma-Aldrich Canada Co.,), the silica nanoparticles do not contain much silanol groups, hence it can be considered as hydrophobic. This can be one of possibilities for the marginal change in the equilibrium contact angle for different silica embedded mats. The silica nanoparticles on the surface of the fibers can act as a barrier to the movement of the contact line and that might be another reason for the difference in the wettability. The change in the equilibrium contact angle might not be a good indicator for this argument. Therefore, the transient variation in the spreading diameter until the drop attains the equilibrium is also analyzed in detail.

3.3.4 Dynamic Water Contact Angle

Similar to an inkjet droplet spreading on a printing paper, when a distill-water drop is deposited on an electrospun hydrophilic mat, the drop will spread and be absorbed by the mat simultaneously [28]. As is illustrated in Figure 3.5, this process can be divided into three stages. First is the relaxation stage, in which the instantaneous spreading results in a sharp decrement in the contact angle and it relaxes towards the equilibrium contact angle θ_E. At the same time, the three-phase contact line separating the wet area from the dry area exponentially increases. For a distill-water drop spreading on electrospun Nylon 6 mats, the first stage is surprisingly long (3 to 5 seconds) comparing to other porous substrates such as paper [24]. After the first stage, the drop has already attained an equilibrium state. However, as can be seen in Figure 3.5, the contact angle is still decreasing with a lower rate. This is the second stage which is the decreasing stage. Since the drop volume is 1 μL which is very low, the evaporation is the main reason accounting for the decreasing phenomenon in this stage. The details of this stage and the effect of solution parameters on this stage will be discussed later. At the end of the decreasing stage, the drop transits to the third stage (vanishing stage) where the contact angle and base diameter are diminishing simultaneously. During this stage, the radius of the remaining drop decreases sharply, and the drop finally

disappeared. A typical dying time for water droplet of 3-5 μL is in the range of 200-500 seconds [87] and in the current experiments, the 1 μL drop vanishes less than 200s after the drop deposition.

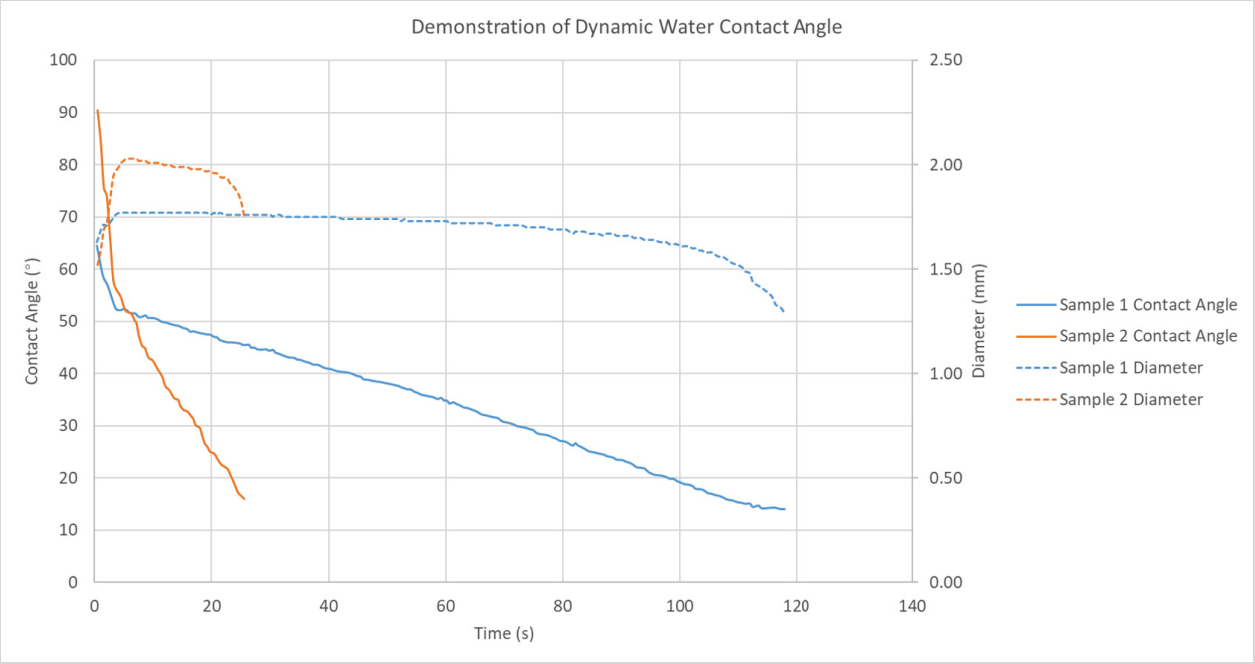

Figure 3.5: A typical wetting of mat: transient variations in the contact angle of water drop

As shown in Figure 3.6, Figure 3.7 and Figure 3.8, when no silica nanoparticles are added, the wetting behavior is similar in all three Nylon 6 concentrations. At the very beginning, they all take around 3 to 5 seconds in the relaxation stage to reach the equilibrium contact angle. Then it decreases continuously until around 3 minutes after the drop deposition. For the mats prepared from all those three solutions, they have similar porosity and in microscopic view they all have smooth long nanofibers. The amount of Nylon 6 that contacts with the water is similar, thus the droplet dying process is almost the same.

For the same Nylon 6 concentration, it can be seen that as silica weight fraction increases, the spreading of the water droplets and decrease in the contact angle is faster. More specifically, the second stage of the transient process shown in Figure 3.5 becomes shorter as silica weight fraction increases. The only exception is N17 samples, in which the curves of S0N17 and S3N17 do not have any significant difference. It can be observed that, higher Nylon 6 concentration will be more sensitive to the silica addition. For example, when 3% of silica is added into solutions with different Nylon 6 concentration, S3N17 still need around

170s to attain the vanishing drop region or unmeasurable region. However, for S3N18.5 and S3N20, they require around 120s and 80s to finish the drop vanishing process respectively. It is more significant when silica weight fraction reaches 9%, as S9N20 only needs 1/3 of the time as compared to the time required by S9N17.

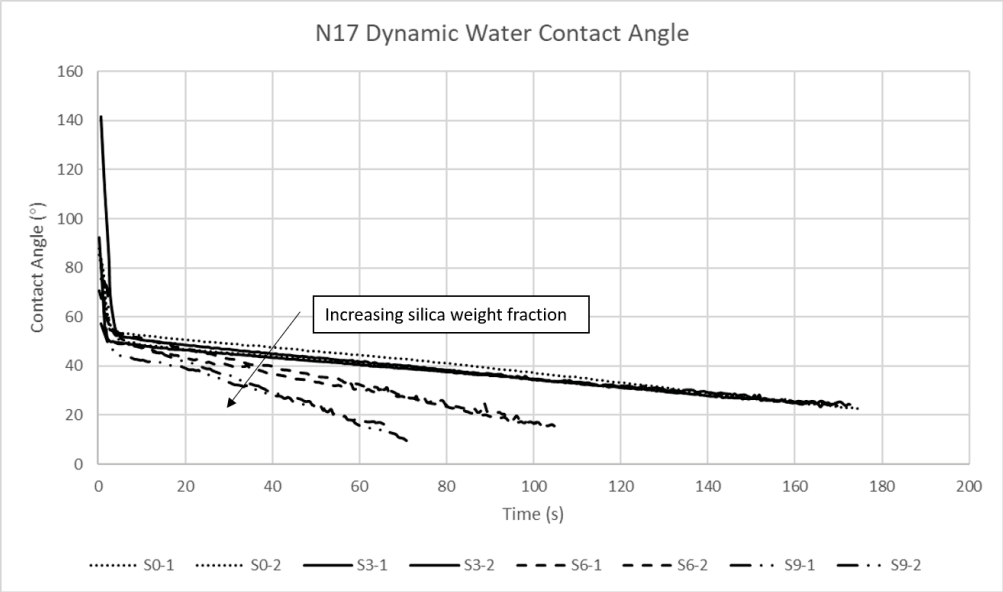

Figure 3.6: Dynamic Water Contact angle of mats made by solutions with 17wt% Nylon 6 concentration

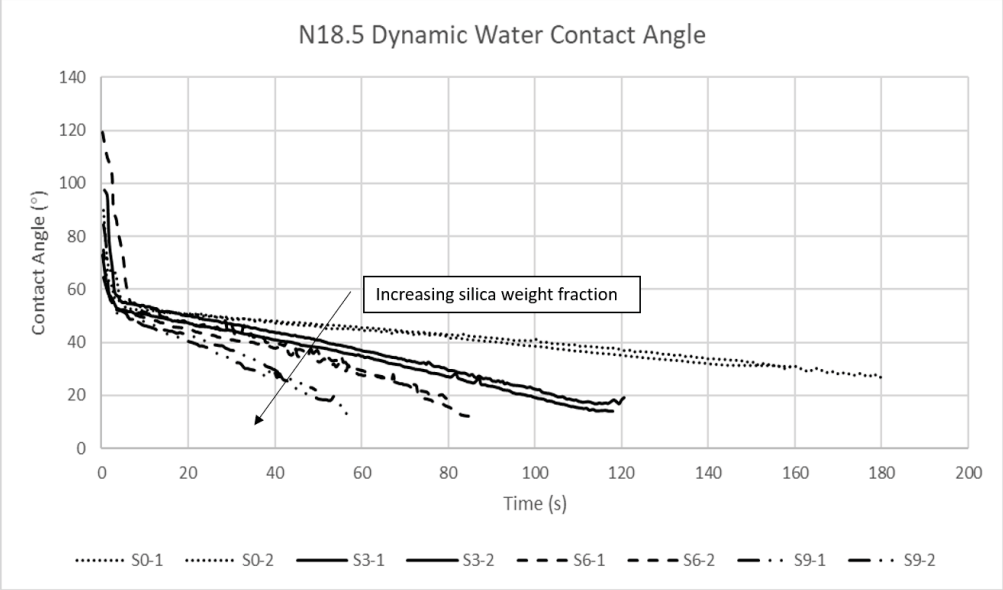

Figure 3.7: Dynamic Water Contact angle of mats made by solutions with 18.5wt% Nylon 6 concentration

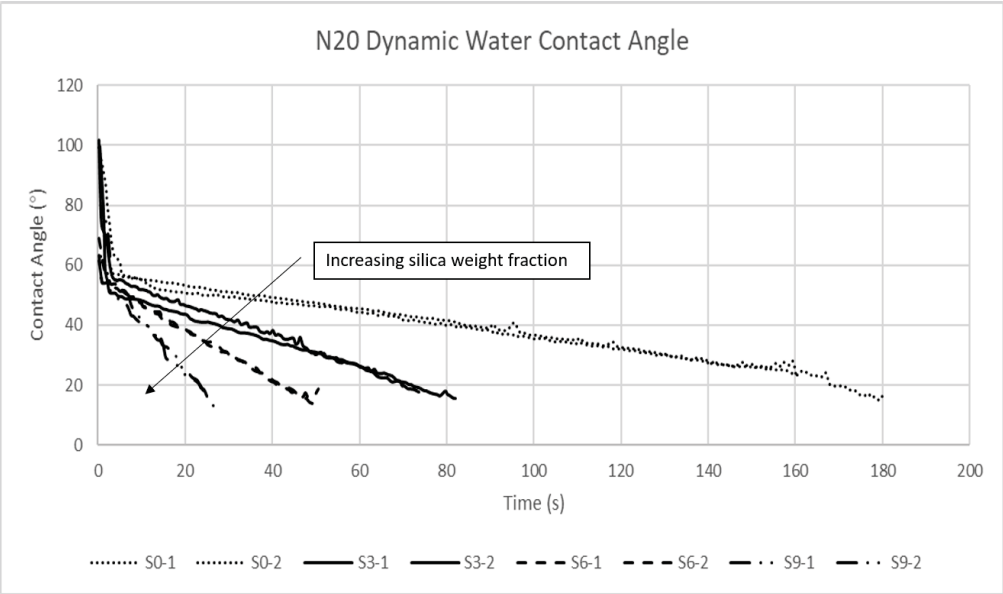

Figure 3.8: Dynamic Water Contact angle of mats made by solutions with 20wt% Nylon 6 concentration

As the volume of the drop, volatility of the drop, ambient temperature and humidity was not changed during the experiments, the silica addition should have no effects on the drop evaporation process. However, the results in Figure 3.6, Figure 3.7, Figure 3.8 revealed that the drop transient process is affected. According to the findings by Ismail et al. [24], the water drop vanishing phenomenon attributes to not only the evaporation process, but also the imbibition of the water drop by the electrospun porous mats. The difference between evaporation and imbibition is the change in the drop diameter or the moving three phase contact line along with the diminishing contact angle. In evaporation process, the majority of the period, the diameter of the drop remains unchanged but if the substrate is reactive or porous, the diameter shrinking is comparable with the decreasing contact angle. To pinpoint this difference, the diameter variation for same volume drops on all the samples are extracted. The diameter variation curves of N20 are shown in Figure 3.9 and for the brevity purpose only N20 samples are shown as representative of all mats. The N17 and N18.5 samples have similar trend. In this figure, for, S0N20 and S3N20 samples, the water drop diameter almost remains unchanged for a period of time and only at the last stage, it decreased sharply until the drop is vanished. It suggests that the evaporation is the main cause of the decreasing contact angle. The difference between S3 and S0 samples is due to the imbibition of water into the mats which can be easily seen in the figure by observing the difference in the change

in the diameter. Also, the addition of silica nanoparticles enhanced the imbibition of the water into the mats. As a result, the drops on S3N20 vanishes quicker than those on S0N20. When silica weight fraction is increased to 6%, the evaporation of the water in the mats is so quick that the water drop is constantly being absorbed into the mats. In this situation, the imbibition of the water drop into the mats also plays a role in the contact angle decreasing phenomenon and this phenomenon is even more prominent when 9% of silica nanoparticles are reinforced. Therefore, it can be concluded that the silica embedment not only controls the evaporation process, but also boost the imbibition process of the water drop.

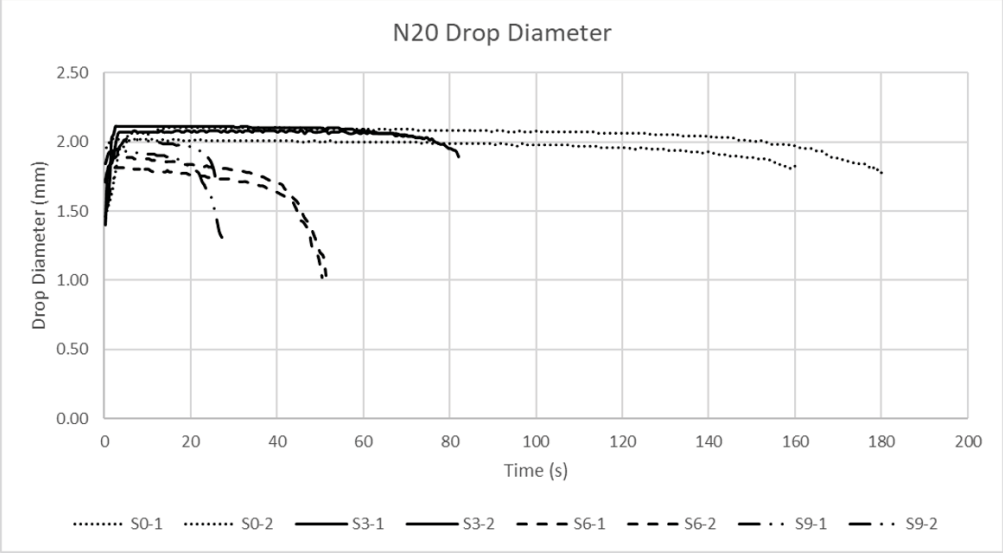

Figure 3.9: Drop diameter variation of N20 samples

The increasing amount of silica nanoparticles creates more micro- and nano-cracks inside the Nylon 6 nanofibers and more spindle-like silica beads are formed. These micro- and nano-cracks allows more Nylon 6 surface asperities at the three-phase contact line. Since Nylon 6 molecules affinity towards water due to the existence of amide groups, additional micro/nano sized sites could facilitate absorption [88]. In addition, the hydrophobic silica nanoparticles allow the water to move easier in the Nylon 6 matrix. That is to say, at the same environmental condition, the water is easy to penetrate in and evaporate out with more silica nanoparticles imbedded. Hence, the evaporation and imbibition process are enhanced in high silica weight fraction samples. In conclusion, the drop vanishing process can be controlled by the silica weight fraction.

3.3.5 Surface Charging Effect

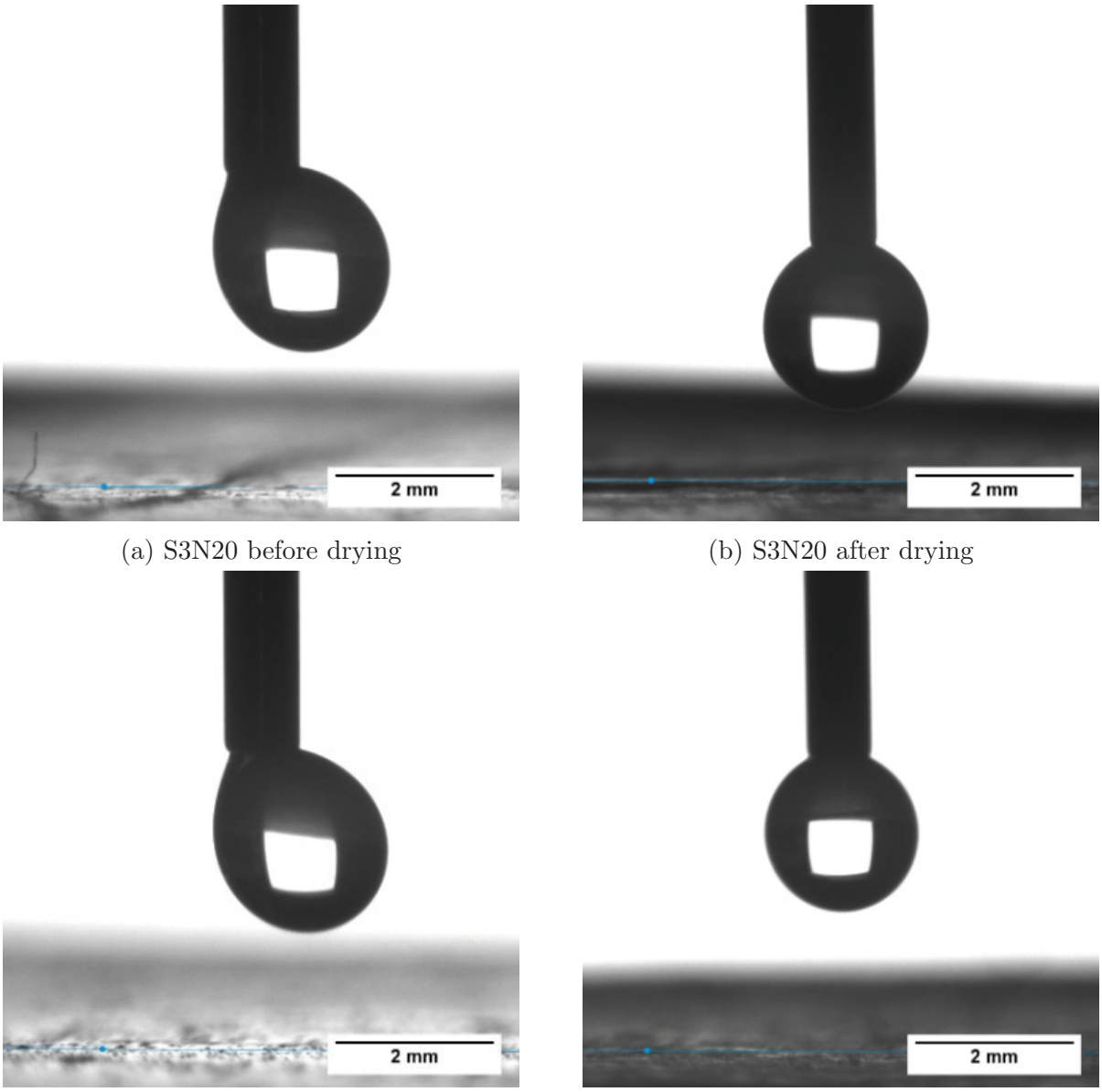

(a) S3N20 before drying

(b) S3N20 after drying

(c) S3N18.5 before drying

(d) S3N18.5 after drying

Figure 3.10: Typical examples of charging effect by residual solvent

It is well documented that the electrospun mat inherently possess charges on the surface [89, 90]. While measuring the contact angle, we observed the role of these charges as depicted in the Figure 3.10. This is the most interesting phenomenon that was observed during the experiment. There are 12 solutions recipes and for each solution recipe, 4 samples were made, *i.e.*, in total 48 samples were fabricated and characterized during the experiment. Although distill-water was used in the experiments, 8 out of the 48 samples showed the effect

of unknown force on the hanging droplet at the tip of the needle. As is shown in Figure 3.10a and 3.10c, water drop starts to deviate from its center line when it brought in the vicinity of the mat. The deviation from the center location of the drop is proportional to the distance between the drop and the mat. When the drop is very close to the mat, it was suddenly attracted by the mat and spread instantaneously. This detachment of the drop from the needle is merely due to this mysterious force between the liquid vapor interface and mat. To delineate the role of this charges on the mat possibly due to the existence of residual solvent inside the electrospun fiber, the mat was purposefully kept in vacuum and dried for a longer period of time (mostly for a day). After this unconventional treatment, this effect was eliminated. Figure 3.10b and 3.10d are the images of drop deposition process on the same mat that showed the drop repellency in Figure 3.10a and 3.10c. The tilting drop returns to normal.

Alternatively, one may argue that the electrospun nanofiber mats is statically charged during the electrospinning process, so it can create a small electric field which is strong enough to attract the water droplet. As can be seen during the electrospinning process, all the samples contain electrostatic charges since they are fibrous mats made from high intensity electrical field. However, the static charges on the surface is not strong enough to cause attraction to the water droplet. The solvent used in this paper, which is 88% formic acid with 12% of water, might also be partially charged under the high intensity electric field. Some charged residual solvents between the nanofiber, along with the static charges on the surface might have caused this drop tilting phenomenon.

Control of this charging effect is not trivial, as there is no paper reported similar phenomenon. However, this can be studied further in detail to pinpoint the role of these charge on different situations. It has been confirmed that the residual formic acid can create such charges on the mat and one can carefully control this residue in the mat and thus the charge on the mat. Detailed analysis and parametric study on the role of these charges in relation with the drop spreading can be an interesting study, which is beyond the scope of our aim.

3.4 Conclusion

In this paper, the tunable wettability of electrospun Nylon 6/silica nanocomposite mats was achieved. Super-thin smooth Nylon 6/silica nanocomposite fibers were obtained. The

average fiber diameter and the silica bead structure were well controlled by tuning the Nylon 6 concentration and silica weight fraction. Surface roughness of the electrospun mats was increased with the increase of silica weight fraction and decrease of Nylon 6 concentration. On the other hand, the porosity of the mats was not significantly affected by both parameters. The wettability of the nanocomposite mats was characterized. The equilibrium contact angle increased by only around 4° when Nylon 6 concentration increased from 17wt% to 20wt%. However, the effect of silica nanoparticle embedment on the contact angle value was limited. In addition, the effect of Nylon 6 concentration and silica weight fraction on the water drop vanishing process was also studied. Both the imbibition and evaporation process were greatly enhanced when silica nanoparticles are added. When silica weight fraction is increased to 9%, only 10% to 30% of the time is needed for the mats produced from the same Nylon 6 concentration to completely vanish the drop. Finally, an interesting surface charging phenomenon was discovered. In some of the electrospun mats, the charged residual solvent inside the mats is able to attract the water drop during the drop deposition process.

Chapter 4

Summary and Future Works

4.1 Summary of the Thesis

Electrospun Nylon 6/Silica mats with nanocomposite fibers were successfully fabricated. The effect of solution parameters on the properties, especially the wettability, of the mat was studied. Based on the detailed analysis the controlled imbibition process was achieved by manipulating the nanocomposite withing fibers. The dependency of the bulk as well as surface properties on the liquid solution parameters is discussed in depth.

In Chapter 2, the selected Nylon 6 concentration with appropriate weight fraction of silica nanoparticles was considered for fabricating bead-free Nylon 6/silica fibrous nanocomposites. The change in the viscosity due to the Nylon 6 concentration and addition of nanoparticles is reported. Then characterizations of obtained nanocomposite mats in both macroscopic view (surface roughness and porosity) and microscopic view (fiber morphology and average fiber diameter) were done. Statistical analysis was applied to the fiber diameter measurements to obtain the effect of Nylon 6 concentration and silica weight fraction on the fiber diameter. In addition, the effect of silica weight fraction on the electrospun mats' nanostructures (silica beads and the spider-net-like nanostructure). The summary of key findings are:

- In the shear rate range of $20s^{-1}$ to $100s^{-1}$, the viscosity of the Nylon 6 - silica/formic acid solutions remains constant. The viscosity of the solutions increased sharply with the rise of Nylon 6 concentration and moderately with the increase of silica weight fraction.

- For the pure Nylon 6 nanofibers, the average fiber diameter increased significantly with the increase of Nylon 6 concentration. This results agree with the viscosity measure-

ment.

- For Nylon 6/silica nanocomposite fibers when the silica weight fraction exceeds the threshold value, the average fiber diameter slightly increased with the addition of silica nanoparticles. This threshold value depends on the fiber diameter of pure Nylon 6 nanofibers.

- Ultra-thin spider-net-like nanostructures are randomly distributed all over the mats. The formation of this nanostructure was due to partially ionization of the amide groups in some regions of the solutions. The random formation of spider-net-like nanostructure morphology and characteristics are independent of both Nylon 6 concentration and silica weight fraction, which needs further attention to pinpoint the rationale of it.

- The porosity of the electrospun mats is not influenced by the Nylon 6 concentration and silica weight fraction.

- Surface roughness increases with the increase of silica weight fraction and decrease of Nylon 6 concentration. In addition, due to the portions with flat or semi-flat fibers within the mats made from N15 solutions, the surface roughness of those mats is significantly higher than others.

In Chapter 3, the solutions' parameters were refined for tunable wettability and spreading analysis. To avoid having those portions with flat or semi-flat fibers, the Nylon 6 concentration was modified accordingly. The silica weight fraction was also refined to 0%, 3%, 6% and 9% to have a better control of silica agglomeration. In addition to the characterization performed in Chapter 2, the dynamics of water droplet spreading is studied.The absorption rate based on the spreading rate of droplet is investigated. The main findings are listed below:

- The average fiber diameter and fiber morphology are well controlled for wetting characteristics.

- Surface roughness and porosity was similar to the mats that were obtained in Chapter 2.

- The variation of equilibrium contact angle by the Nylon 6 concentration was simple. The equilibrium contact angle increased with the increase of Nylon 6 concentration. However, the variation of equilibrium contact angle by the silica addition was different. Apart from chemical inhomogeneity, the surface roughness played a more important role than the silica inherent hydrophobicity.

- With approximately constant equilibrium angle, the imbibtition rates were altered by merely changing the reinforcement of the nanoparticles .

- Surprisingly, it was found that some of the charged electrospun mats are able to attract the distilled-water drops. The charging effect is due to the residual solvent that was left in the mats during the electrospinning process.

In addition, the results of the fiber diameter measurements can be summarized. The average fiber diameter of pure Nylon 6 nanofibers is increased with the increasing of Nylon 6 concentration. As Nylon 6 concentration increases, the viscosity of the solutions increased thus the elongation process becomes harder. Therefore, the fiber diameter is increased with the increase of Nylon 6 concentration.

4.2 Future Works

1. **Verification of the dispersion of silica nanoparticles**

   In this project, the dispersion of silica nanoparticles within the Nylon 6/formic acid solution is only verified by the SEM images of the end products. So before the electrospinning process, how well the silica nanoparticles are dispersed within the solution is unknown. In furture works, the dispersion of the silica within the solution can actually be verified by dynamic light scattering.

2. **Investigation on the Threshold Values and Critical Values**

   As mentioned in Chapter 2, there is a threshold value of silica weight fraction beyond which the fiber diameters will increase with the increase of silica weight fraction. This threshold criteria depends on Nylon 6 concentration and it can only be determined by refining the grid of silica weight fraction in a fixed Nylon 6 concentration. Also, the critical value that the agglomerated silica beads will form can also be determined by

experiment. As a continuation of this work, a design curve can be provided for the fabrication of fibrous Nylon 6/silica nanocomposites.

3. **Application of Fibrous Nylon 6/silica Nanocomposites in Solid-phase Micro-extraction**

   Nylon 6 bulk material was reinforced by silica nanoparticles and used as sorbent for solid-phase micro-extraction. In Chapter 3, it can be seen that the wettability of electrospun Nylon 6/silica nanocomposites can be easily controlled which can make it an ideal candidate for for solid-phase micro-extraction. Future work can be devoted to fabricate ideal electrospun fibrous Nylon 6/silica nanocomposites for the use of solid-phase micro-extraction.

4. **Application of Electrospinning Technique in the Dielectric Coating for Electrowetting**

   Electrowetting is a rapid and reversible technique to tune the wettability of a substrate [91]. The substrates used in electrowetting studies are usually conductive metals coated with dielectric polymers[92]. Currently, spin coating is used as the fabrication method for the dielectric polymer coating[93]. As can be seen in the current work, electrospinning can be an alternative method for the polymer coating. Primarily, the wettability of the coating can be directly controlled by tuning the electrospinning processing parameters. The work done in this thesis can be used as a guidance for this purpose. Secondly, for hydrophobic polymers, fibrous materials could increase the surface roughness of the coating. As a result, the contact angle will be increased thus the electrowetting phenomenon might also be more significant. Last but not least, the effect of charges on drop demonstrated in Chapter 3 reveals that the fibrous structure might have inherent charges which need to be investigated in detail. Based on this, one can agree, there is a potential in pursuing the research on the topic of electric/dielectric property of the electrospun mats.

References

[1] C. J. Luo, Simeon D. Stoyanov, E. Stride, E. Pelan, and M. Edirisinghe. Electrospinning versus fibre production methods: from specifics to technological convergence. *Chemical Society Reviews*, 41(13):4708, 2012. ISSN 0306-0012. doi: 10.1039/c2cs35083a. URL `http://xlink.rsc.org/?DOI=c2cs35083a`.

[2] Zheng Ming Huang, Y. Z. Zhang, M. Kotaki, and S. Ramakrishna. A review on polymer nanofibers by electrospinning and their applications in nanocomposites. *Composites Science and Technology*, 63(15):2223–2253, 2003. ISSN 02663538. doi: 10.1016/S0266-3538(03)00178-7.

[3] T. and C. Joachim. Drawing a single nanofibre over hundreds of Ondarçuhumicrons. *Europhysics Letters*, 42(2):215–220, 1998. ISSN 02955075. doi: 10.1209/epl/i1998-00233-9.

[4] Guojun Liu, Jianfu Ding, Lijie Qiao, Andrew Guo, Boris P. Dymov, James T. Gleeson, T. Hashimoto, and K. Saijo. Polystyrene - block - poly (2 - cinnamoylethyl methacrylate) Nanofibers - Preparation , Characterization , and Liquid Crystalline Properties. *Chemistry - A European Journal*, 5(9):2740–2749, 1999. doi: http://dx.doi.org/10.1002/(SICI)1521-3765(19990903)5:9⟨2740::AID-CHEM2740⟩3.0.CO;2-V.

[5] W E Teo and S Ramakrishna. A review on electrospinning design and nanofibre assemblies. *Nanotechnology*, 17(14):R89–R106, 2006. ISSN 0957-4484. doi: 10.1088/0957-4484/17/14/R01.

[6] J Wu, N Wang, Y Zhao, and L Jiang. Electrospinning of multilevel structured functional micro-/nanofibers and their applications. *Journal of Materials Chemistry A*, 1(25):7290–7305, 2013. ISSN 2050-7488. doi: Doi10.1039/C3ta10451f.

[7] Seeram Ramakrishna. *Introduction To Electrospinning And Nanofibers*. Hackensack, NJ: World Scientific, 2005.

[8] John F Cooley. Apparatus for electrically dispersing fluids, Feb 1902.

[9] Anton Formhals. Process and apparatus for preparing artificial threads, Oct 1934.

[10] Thandavamoorthy Subbiah, G. S. Bhat, R. W. Tock, S. Parameswaran, and S. S. Ramkumar. Electrospinning of nanofibers. *Journal of Applied Polymer Science*, 96(2):557–569, 2005. ISSN 00218995. doi: 10.1002/app.21481.

[11] von Stefan Leonhardt. Formation and characterization of composite nanofibers for antimicrobial applications. Master's thesis, am Lehrstuhl für Medizintechnik der TU München, 2014.

[12] J. Doshi and D.H. Reneker. Electrospinning process and applications of electrospun fibers. *Conference Record of the 1993 IEEE Industry Applications Conference Twenty-Eighth IAS Annual Meeting*, 35:151–160, 1995. ISSN 03043886. doi: 10.1109/IAS.1993.299067.

[13] Electrospinning, June 2018. URL `https://www.scopus.com/`.

[14] Seema Agarwal Joachim H. Wendorff and Andreas Greiner. *Electrospinning Materials, Processing, and Applications*. Wiley-VCH Verlag & Co. KGaA, Boschstr. 12, 69469 Weinheim, Germany, 2012.

[15] Feng Pan. Design guidance for electrospun nylon 6 nanofiber morphology through design of experiment and statistical analysis method and mechanical properties characterization. Master's thesis, University of Alberta, 2014.

[16] Darunee Aussawasathien. *Electrospun Conducting Nanofiber–Based Materials and Their Characterizations: Effects Of Fiber Characteristics On Properties And Applications*. PhD thesis, University of Akron, 2006.

[17] Ashwini Wali, Yucheng Zhang, Poulomi Sengupta, Yuji Higaki, Atsushi Takahara, and Manohar V. Badiger. Electrospinning of non-ionic cellulose ethers/polyvinyl alcohol nanofibers: Characterization and applications. *Carbohydrate Polymers*, 181(July 2017):

175–182, 2018. ISSN 01448617. doi: 10.1016/j.carbpol.2017.10.070. URL https://doi.org/10.1016/j.carbpol.2017.10.070.

[18] Najmeh Moazeni, Ali Akbar Merati, Masoud Latifi, Mehdi Sadrjahani, and Shohre Rouhani. Fabrication and characterization of polydiacetylene supramolecules in electrospun polyvinylidene fluoride nanofibers with dual colorimetric and piezoelectric responses. *Polymer (United Kingdom)*, 134:211–220, 2018. ISSN 00323861. doi: 10.1016/j.polymer.2017.11.063.

[19] Ren Hui Zhang, Juan Zhao, and Jun Liang. A novel multifunctional PTFE/PEO composite coating prepared by one-step method. *Surface and Coatings Technology*, 299:90–95, 2016. ISSN 02578972. doi: 10.1016/j.surfcoat.2016.05.001. URL http://dx.doi.org/10.1016/j.surfcoat.2016.05.001.

[20] R. Nirmala, Jin Won Jeong, Hyun Ju Oh, R. Navamathavan, Mohamed El-Newehy, Salem S. Al-Deyab, and Hak Yong Kim. Electrical properties of ultrafine nylon-6 nanofibers prepared via electrospinning. *Fibers and Polymers*, 12(8):1021–1024, 2011. ISSN 12299197. doi: 10.1007/s12221-011-1021-4.

[21] Hem Raj Pant, Ki Taek Nam, Hyun Ju Oh, Gopal Panthi, Hee Dong Kim, Byung Il Kim, and Hak Yong Kim. Effect of polymer molecular weight on the fiber morphology of electrospun mats. *Journal of Colloid and Interface Science*, 364(1):107–111, 2011. ISSN 00219797. doi: 10.1016/j.jcis.2011.07.094. URL http://dx.doi.org/10.1016/j.jcis.2011.07.094.

[22] Chunlei Su, Yuping Li, Youzhi Dai, Fang Gao, Kexin Tang, and Hongbin Cao. Fabrication of three-dimensional superhydrophobic membranes with high porosity via simultaneous electrospraying and electrospinning. *Materials Letters*, 170:67–71, 2016. ISSN 18734979. doi: 10.1016/j.matlet.2016.01.133. URL http://dx.doi.org/10.1016/j.matlet.2016.01.133.

[23] Bharat Bhushan and Yong Chae Jung. Wetting study of patterned surfaces for superhydrophobicity. *Ultramicroscopy*, 107(10-11):1033–1041, 2007. ISSN 03043991. doi: 10.1016/j.ultramic.2007.05.002.

[24] Md Farhad Ismail Aleksey Baldygin Thomas Willers Prashant R. Waghmare. Optical contact angle measurement considering spreading, evaporation and reactive substrate. *Advances in Contact Angle, Wettability and Adhesion*, 3:59–80, 2018.

[25] Waqi Donaldson, Erle C.; Alam. *Wettability*. Gulf Publishing Company, 2008.

[26] S. Baxter A. B. D. Cassie. Wettability of porous surface. *Physics and Chemistry of Surfaces*, 1944.

[27] Abraham Marmur. Wetting on hydrophobic rough surfaces: To be heterogeneous or not to be? *Langmuir*, 19(20):8343–8348, 2003. ISSN 07437463. doi: 10.1021/la0344682.

[28] Andrew Clarke, T. D. Blake, K. Carruthers, and A. Woodward. Spreading and imbibition of liquid droplets on porous surfaces. *Langmuir*, 18(8):2980–2984, 2002. ISSN 07437463. doi: 10.1021/la0117810.

[29] Bodil. Bracco, Gianangelo. Holst. *Surface science techniques*. Berlin: Springer, 2013.

[30] Susannah Handley. *Nylon: the story of a fashion revolution : a celebration of design from art silk to nylon and thinking fibres*. Baltimore, Md: Johns Hopkins University Press, 1999.

[31] J. E. McIntyre. *Synthetic Fibres: Nylon, Polyester, Acrylic, Polyolefin*. CRC Press, 2005.

[32] Edward S Wheeler, Ambler, and Charles A Signorino. Nylon solvent and method of making same, May 1968.

[33] Md Shahidul Islam, Jeffrey R. McCutcheon, and Md Saifur Rahaman. A high flux polyvinyl acetate-coated electrospun nylon 6/SiO2composite microfiltration membrane for the separation of oil-in-water emulsion with improved antifouling performance. *Journal of Membrane Science*, 537(February):297–309, 2017. ISSN 18733123. doi: 10.1016/j.memsci.2017.05.019.

[34] Bishweshwar Pant, Hem Raj Pant, Dipendra Raj Pandeya, Gopal Panthi, Ki Taek Nam, Seong Tshool Hong, Cheol Sang Kim, and Hak Yong Kim. Characterization

and antibacterial properties of Ag NPs loaded nylon-6 nanocomposite prepared by one-step electrospinning process. *Colloids and Surfaces A: Physicochemical and Engineering Aspects*, 395:94–99, 2012. ISSN 09277757. doi: 10.1016/j.colsurfa.2011.12.011. URL http://dx.doi.org/10.1016/j.colsurfa.2011.12.011.

[35] Nor Dalila Nor Affandi, Yen Bach Truong, Illias Louis Kyratzis, Rajiv Padhye, and Lyndon Arnold. Fabrication and characterisation of hydrophobic and hydrophilic nanofibrous membranes. *2010 International Conference on Science and Social Research (CSSR 2010)*, (Cssr):789–794, 2010. doi: 10.1109/CSSR.2010.5773893. URL http://ieeexplore.ieee.org/lpdocs/epic03/wrapper.htm?arnumber=5773893.

[36] Bin Ding, Jinyou Lin, Xianfeng Wang, Jianyong Yu, Jianmao Yang, and Yu Cai. Investigation of silica nanoparticle distribution in nanoporous polystyrene fibers. *Soft Matter*, 7(18):8376–8383, 2011. ISSN 1744-683X. doi: 10.1039/C1SM05791J.

[37] Yanhuai Ding, Ping Zhang, Yong Jiang, Fu Xu, Jiuren Yin, and Yongde Zuo. Mechanical properties of nylon-6/SiO2 nanofibers prepared by electrospinning. *Materials Letters*, 63(1):34–36, 2009. ISSN 0167577X. doi: 10.1016/j.matlet.2008.08.058.

[38] R. Nirmala, R. Navamathavan, Soo Jin Park, and Hak Yong Kim. Recent Progress on the Fabrication of Ultrafine Polyamide-6 Based Nanofibers Via Electrospinning: A Topical Review. *Nano-Micro Letters*, 6(2):89–107, 2014. ISSN 21505551. doi: 10.1007/BF03353773.

[39] Quan Shi, Narendiran Vitchuli, Joshua Nowak, Jesse Noar, Jane M. Caldwell, Frederick Breidt, Mohamed Bourham, Marian McCord, and Xiangwu Zhang. One-step synthesis of silver nanoparticle-filled nylon 6 nanofibers and their antibacterial properties. *Journal of Materials Chemistry*, 21(28):10330, 2011. ISSN 0959-9428. doi: 10.1039/c1jm11492a. URL http://xlink.rsc.org/?DOI=c1jm11492a.

[40] Kuitian Tan and S. Kay Obendorf. Fabrication and evaluation of electrospun nanofibrous antimicrobial nylon 6 membranes. *Journal of Membrane Science*, 305(1-2):287–298, 2007. ISSN 03767388. doi: 10.1016/j.memsci.2007.08.015.

[41] Hem Raj Pant, Chan Hee Park, Leonard D. Tijing, Altangerel Amarjargal, Do Hee Lee, and Cheol Sang Kim. Bimodal fiber diameter distributed graphene oxide/nylon-6 com-

posite nanofibrous mats via electrospinning. *Colloids and Surfaces A: Physicochemical and Engineering Aspects*, 407:121–125, 2012. ISSN 18734359. doi: 10.1016/j.colsurfa.2012.05.018. URL http://dx.doi.org/10.1016/j.colsurfa.2012.05.018.

[42] Abdalla Abdal-hay, Leonard D Tijing, and Jae Kyoo. Characterization of the surface biocompatibility of an electrospun nylon 6 / CaP nanofiber scaffold using osteoblasts. *Chemical Engineering Journal*, 215-216:57–64, 2013. ISSN 1385-8947. doi: 10.1016/j.cej.2012.10.046. URL http://dx.doi.org/10.1016/j.cej.2012.10.046.

[43] Abdalla Abdal-Hay, Hem Raj Pant, and Jae Kyoo Lim. Super-hydrophilic electrospun nylon-6/hydroxyapatite membrane for bone tissue engineering. *European Polymer Journal*, 49(6):1314–1321, 2013. ISSN 00143057. doi: 10.1016/j.eurpolymj.2013.02.004. URL http://dx.doi.org/10.1016/j.eurpolymj.2013.02.004.

[44] Haitao Zhang, Chengyao Wu, and Yunlong Zhang. Elaboration , characterization and study of a novel affinity membrane made from electrospun hybrid chitosan / nylon-6 nanofibers for papain purification. pages 2296–2304, 2010. doi: 10.1007/s10853-009-4191-3.

[45] Seongpil An, Min Wook Lee, Bhavana N. Joshi, Ayeong Jo, Jinho Jung, and Sam S. Yoon. Water purification and toxicity control of chlorophenols by 3D nanofiber membranes decorated with photocatalytic titania nanoparticles. *Ceramics International*, 40(2):3305–3313, 2014. ISSN 02728842. doi: 10.1016/j.ceramint.2013.09.104. URL http://dx.doi.org/10.1016/j.ceramint.2013.09.104.

[46] Mozhdeh Ghani, Ali Akbar Gharehaghaji, Mokhtar Arami, Negar Takhtkuse, and Babak Rezaei. Fabrication of electrospun polyamide-6/chitosan nanofibrous membrane toward anionic dyes removal. *Journal of Nanotechnology*, 2014, 2014. ISSN 16879511. doi: 10.1155/2014/278418.

[47] Palanisamy Manivasakan, N.R. Dhineshbabu, and Venkatachalam Rajendran. Hydrophobic and thermal behaviour of nylon 6 nanofibre web deposited on cotton fabric through electrospinning. *Micro & Nano Letters*, 9(8):519–522, 2014. ISSN 1750-0443. doi: 10.1049/mnl.2014.0161. URL http://digital-library.theiet.org/content/journals/10.1049/mnl.2014.0161.

[48] Hem Raj Pant and Cheol Sang Kim. Electrospun gelatin/nylon-6 composite nanofibers for biomedical applications. *Polymer International*, 62(7):1008–1013, 2013. ISSN 09598103. doi: 10.1002/pi.4380.

[49] Hem Raj Pant, Bishweshwar Pant, Chan Hee Park, Han Joo Kim, Dong Su Lee, Leonard D. Tijing, Bo Sang Hwang, Hak Yong Kim, and Cheol Sang Kim. RGO/Nylon-6 composite mat with unique structural features and electrical properties obtained from electrospinning and hydrothermal process. *Fibers and Polymers*, 14(6):970–975, 2013. ISSN 12299197. doi: 10.1007/s12221-013-0970-1.

[50] Hem Raj Pant, Han Joo Kim, Lok Ranjan Bhatt, Mahesh Kumar Joshi, Eun Kyo Kim, Jeong In Kim, Abdalla Abdal-Hay, K. S. Hui, and Cheol Sang Kim. Chitin butyrate coated electrospun nylon-6 fibers for biomedical applications. *Applied Surface Science*, 285(PARTB):538–544, 2013. ISSN 01694332. doi: 10.1016/j.apsusc.2013.08.089. URL `http://dx.doi.org/10.1016/j.apsusc.2013.08.089`.

[51] Hem Raj Pant, Woo Il Baek, Ki Taek Nam, In Soo Jeong, Nasser A M Barakat, and Hak Yong Kim. Effect of lactic acid on polymer crystallization chain conformation and fiber morphology in an electrospun nylon-6 mat. *Polymer*, 52(21):4851–4856, 2011. ISSN 00323861. doi: 10.1016/j.polymer.2011.08.059. URL `http://dx.doi.org/10.1016/j.polymer.2011.08.059`.

[52] Hem Raj Pant, Madhab Prasad Bajgai, Chuan Yi, R. Nirmala, Ki Taek Nam, Woo Il Baek, and Hak Yong Kim. Effect of successive electrospinning and the strength of hydrogen bond on the morphology of electrospun nylon-6 nanofibers. *Colloids and Surfaces A: Physicochemical and Engineering Aspects*, 370(1-3):87–94, 2010. ISSN 09277757. doi: 10.1016/j.colsurfa.2010.08.051. URL `http://dx.doi.org/10.1016/j.colsurfa.2010.08.051`.

[53] Iler Ralph K Ralph K. Iler. *The Chemistry of Silica: Solubility, Polymerization, Colloid and Surface Properties and Biochemistry of Silica*. Wiley, 1979.

[54] Juan. Vivero-Escoto. *Silica nanoparticles: preparation, properties, and uses*. New York: Nova Science Publishers, 2012.

[55] Ozcan Koysuren and H. Nagehan Koysuren. Characterization of poly(methyl methacrylate) nanofiber mats by electrospinning process. *Journal of Macromolecular Science, Part A*, 53(11):691–698, 2016. ISSN 1060-1325. doi: 10.1080/10601325.2016.1224627. URL https://www.tandfonline.com/doi/full/10.1080/10601325.2016.1224627.

[56] Shaohua Jin, Y. Park, and Chung Hee Park. Preparation of breathable and superhydrophobic polyurethane electrospun webs with silica nanoparticles. *Textile Research Journal*, 2015. ISSN 0040-5175. doi: 10.1177/0040517515617417. URL http://trj.sagepub.com/cgi/doi/10.1177/0040517515617417.

[57] Yuan Liao, Miao Tian, and Rong Wang. A high-performance and robust membrane with switchable super-wettability for oil/water separation under ultralow pressure. *Journal of Membrane Science*, 543(June):123–132, 2017. ISSN 18733123. doi: 10.1016/j.memsci.2017.08.056. URL http://dx.doi.org/10.1016/j.memsci.2017.08.056.

[58] E. M. Reyes-Gallardo, R. Lucena, and S. Cárdenas. Silica nanoparticles–nylon 6 composites: synthesis, characterization and potential use as sorbent. *RSC Adv.*, 7 (4):2308–2314, 2017. ISSN 2046-2069. doi: 10.1039/C6RA24739C. URL http://xlink.rsc.org/?DOI=C6RA24739C.

[59] Ali Aghakhani, Ensiyeh Kazemi, and Mahmood Kazemzad. Preparation of a novel KCC-1/nylon 6 nanocomposite via electrospinning technique. *Journal of Nanoparticle Research*, 17(10):1–13, 2015. ISSN 1572896X. doi: 10.1007/s11051-015-3190-3.

[60] Negar Ghochaghi, Adetoun Taiwo, Matthew Winkel, Brandon Dodd, Karla Mossi, and Gary Tepper. Electrospun polystyrene coatings with tunable wettability. *Journal of Applied Polymer Science*, 132(10):1–6, 2015. ISSN 10974628. doi: 10.1002/app.41592.

[61] Sheikh Rasel and Ghaus Rizvi. Fabrication and Characterization of Electrospun PVA/Mica Fibrous Nanocomposite Mats. *Polymer - Plastics Technology and Engineering*, 57(4):320–326, 2018. ISSN 15256111. doi: 10.1080/03602559.2017.1326137. URL https://doi.org/10.1080/03602559.2017.1326137.

[62] Adeleh Ebrahimi, Mohammad Karimi, and Farzin Zokaee Ashtiani. Characterization of triple electrospun layers of PVDF for direct contact membrane distillation process. *Journal of Polymer Research*, 25(2), 2018. ISSN 15728935. doi: 10.1007/s10965-017-1437-7.

[63] Han Joo Kim, Hem Raj Pant, Altangerel Amarjargal, and Cheol Sang Kim. Incorporation of silver-loaded ZnO rods into electrospun nylon-6 spider-web-like nanofibrous mat using hydrothermal process. *Colloids and Surfaces A: Physicochemical and Engineering Aspects*, 434:49–55, 2013. ISSN 18734359. doi: 10.1016/j.colsurfa.2013.05.038. URL http://dx.doi.org/10.1016/j.colsurfa.2013.05.038.

[64] Jean S. Stephens, D. Bruce Chase, and John F. Rabolt. Effect of the Electrospinning Process on Polymer Crystallization Chain Conformation in Nylon-6 and Nylon-12. *Macromolecules*, 37(3):877–881, 2004. ISSN 0024-9297. doi: 10.1021/ma0351569. URL http://pubs.acs.org/doi/abs/10.1021/ma0351569.

[65] Yu Ying Kuo, Francesca Camilla Bruno, and Jing Wang. Filtration performance against nanoparticles by electrospun nylon-6 media containing ultrathin nanofibers. *Aerosol Science and Technology*, 48(12):1332–1344, 2014. ISSN 15217388. doi: 10.1080/02786826.2014.985782.

[66] Fang Li, Qiming Li, and Hern Kim. Spray deposition of electrospun TiO2 nanoparticles with self-cleaning and transparent properties onto glass. *Applied Surface Science*, 276:390–396, 2013. ISSN 01694332. doi: 10.1016/j.apsusc.2013.03.103. URL http://dx.doi.org/10.1016/j.apsusc.2013.03.103.

[67] Hem Raj Pant, Madhab Prasad Bajgai, Ki Taek Nam, Yun A. Seo, Dipendra Raj Pandeya, Seong Tshool Hong, and Hak Yong Kim. Electrospun nylon-6 spider-net like nanofiber mat containing TiO2 nanoparticles: A multifunctional nanocomposite textile material. *Journal of Hazardous Materials*, 185(1):124–130, 2011. ISSN 03043894. doi: 10.1016/j.jhazmat.2010.09.006. URL http://dx.doi.org/10.1016/j.jhazmat.2010.09.006.

[68] Zhi Liu, Jiang Hui Zhao, Peng Liu, and Ji Huan He. Tunable surface morphology of electrospun PMMA fiber using binary solvent. *Applied Surface Science*, 364:516–521, 2016. ISSN 01694332. doi: 10.1016/j.apsusc.2015.12.176. URL http://dx.doi.org/10.1016/j.apsusc.2015.12.176.

[69] Xi Xiong, Qiang Li, Xu Cheng Zhang, Li Wang, Zhao Xia Guo, and Jian Yu. Poly(vinylidene fluoride)/silica nanocomposite membranes by electrospinning. *Jour-*

nal of Applied Polymer Science, 129(3):1089–1095, 2013. ISSN 00218995. doi: 10.1002/app.38787.

[70] Tewodros Asefa and Zhimin Tao. Biocompatibility of mesoporous silica nanoparticles. *Chemical Research in Toxicology*, 25(11):2265–2284, 2012. ISSN 0893228X. doi: 10.1021/tx300166u.

[71] Q. Shi, N. Vitchuli, J. Nowak, M. McCord, M. Bourham, and X. Zhang. Nylon 6/silica composite and porous nylon 6 nanofibers prepared by electrospinning. *Fiber Society 2009 Fall Meeting and Technical Conference*, pages 2–3, 2009.

[72] R J Going, D E Sameoto, and C Ayranci. Cellulose Nanocrystals: Dispersion in Co-Solvent Systems and Effects on Electrospun Polyvinylpyrrolidone Fiber Mats. *Journal of Engineered Fibers and Fabrics*, 10(3):155–163, 2015. ISSN 15589250.

[73] Sujiao Cao, Fang Qiu, Chen Xiong, Xiaojun Wang, Gang Zhang, Shengru Long, and Jie Yang. Superhydrophobic PES/PDA/ODTS fibrous mat prepared by electrospinning and silanization modification for oil/water separation. *Journal of Applied Polymer Science*, 135(12):1–8, 2018. ISSN 10974628. doi: 10.1002/app.45923.

[74] Bin Ding, Chunrong Li, Yasuhiro Miyauchi, Oriha Kuwaki, and Seimei Shiratori. Formation of novel 2D polymer nanowebs via electrospinning. *Nanotechnology*, 17(15):3685–3691, 2006. ISSN 0957-4484. doi: 10.1088/0957-4484/17/15/011. URL `http://stacks.iop.org/0957-4484/17/i=15/a=011?key=crossref.e0b45e52a01efe3de2b4e014f8ac66a7`.

[75] Samuel Chigome and Nelson Torto. Electrospun nanofiber-based solid-phase extraction. *TrAC Trends in Analytical Chemistry*, 38:21–31, 2012. ISSN 01659936. doi: 10.1016/j.trac.2012.04.011. URL `http://linkinghub.elsevier.com/retrieve/pii/S0165993612001793`.

[76] Han Joo Kim, Hem Raj Pant, Chan Hee Park, Leonard D. Tijing, Nag Jung Choi, and Cheol Sang Kim. Hydrothermal growth of mop-brush-shaped ZnO rods on the surface of electrospun nylon-6 nanofibers. *Ceramics International*, 39(3):3095–3102, 2013. ISSN 02728842. doi: 10.1016/j.ceramint.2012.09.089. URL `http://dx.doi.org/10.1016/j.ceramint.2012.09.089`.

[77] Minsung Kang, Rira Jung, Hun S. Kim, and Hyoung Joon Jin. Preparation of superhydrophobic polystyrene membranes by electrospinning. *Colloids and Surfaces A: Physicochemical and Engineering Aspects*, 313-314:411–414, 2008. ISSN 09277757. doi: 10.1016/j.colsurfa.2007.04.122.

[78] Jianfen Zheng, Aihua He, Junxing Li, Jian Xu, and Charles C. Han. Studies on the controlled morphology and wettability of polystyrene surfaces by electrospinning or electrospraying. *Polymer*, 47(20):7095–7102, 2006. ISSN 00323861. doi: 10.1016/j.polymer.2006.08.019.

[79] Zhengping Zhou and Xiang Fa Wu. Electrospinning superhydrophobic-superoleophilic fibrous PVDF membranes for high-efficiency water-oil separation. *Materials Letters*, 160:423–427, 2015. ISSN 18734979. doi: 10.1016/j.matlet.2015.08.003. URL `http://dx.doi.org/10.1016/j.matlet.2015.08.003`.

[80] Martin K. Dufficy, Mackenzie T. Geiger, Christopher A. Bonino, and Saad A. Khan. Electrospun Ultrafine Fiber Composites Containing Fumed Silica: From Solution Rheology to Materials with Tunable Wetting. *Langmuir*, 31(45):12455–12463, 2015. ISSN 15205827. doi: 10.1021/acs.langmuir.5b03545.

[81] Zhanjian Liu, Huaiyuan Wang, Enqun Wang, Xiguang Zhang, Ruixia Yuan, and Yanji Zhu. Superhydrophobic poly(vinylidene fluoride) membranes with controllable structure and tunable wettability prepared by one-step electrospinning. *Polymer (United Kingdom)*, 82:105–113, 2016. ISSN 00323861. doi: 10.1016/j.polymer.2015.11.045. URL `http://dx.doi.org/10.1016/j.polymer.2015.11.045`.

[82] Manohar Kakunuri, Nandula D Wanasekara, Chandra S Sharma, Mudrika Khandelwal, and Stephen J Eichhorn. Three-dimensional electrospun micropatterned cellulose acetate nanofiber surfaces with tunable wettability. 44709:1–7, 2017. doi: 10.1002/app.44709.

[83] K. Srinivasan. *Composite Materials: production, properties, testing and applications*. Oxford: Alpha Science Intl. Ltd, 2009.

[84] Junhee Choi, Yong Sub Shim, Cheol Hwee Park, Ha Hwang, Jin Ho Kwack, Dong Jun Lee, Young Wook Park, and Byeong Kwon Ju. Junction-Free Electrospun Ag Fiber

Electrodes for Flexible Organic Light-Emitting Diodes. *Small*, 14(7):1–7, 2018. ISSN 16136829. doi: 10.1002/smll.201702567.

[85] Razieh Beigmoradi, Abdolreza Samimi, and Davod Mohebbi-Kalhori. Fabrication of polymeric nanofibrous mats with controllable structure and enhanced wetting behavior using one-step electrospinning. *Polymer (United Kingdom)*, 143:271–280, 2018. ISSN 00323861. doi: 10.1016/j.polymer.2018.04.025. URL https://doi.org/10.1016/j.polymer.2018.04.025.

[86] Mohammad Hossein Azarian, Wan Ahmad Kamil Mahmood, Eunice Kwok, Wan Farahhanim Bt Wan Fathilah, and Nor Fazilah Binti Ibrahim. Nanoencapsulation of intercalated montmorillonite-urea within PVA nanofibers: Hydrogel fertilizer nanocomposite. *Journal of Applied Polymer Science*, 135(10):1–10, 2018. ISSN 10974628. doi: 10.1002/app.45957.

[87] Yuri O. Popov. Evaporative deposition patterns: Spatial dimensions of the deposit. *Physical Review E - Statistical, Nonlinear, and Soft Matter Physics*, 71(3):1–17, 2005. ISSN 15393755. doi: 10.1103/PhysRevE.71.036313.

[88] Sayda M Ibrahim, Amal A El-naggar, Sahar S El Sayed, Sayda M Ibrahim, Amal A El-naggar, Sahar S El, and Sayed Dyestuffs. Dyestuffs and metal ions absorbents based on UV- coated Nylon-6 fabric. *The Journal of The Textile Institute*, 5000:1–7, 2018. ISSN 0040-5000. doi: 10.1080/00405000.2017.1355632. URL https://doi.org/10.1080/00405000.2017.1355632.

[89] Ajay Jagadale, Xuan Zhou, Douglas Blaisdell, and Sen Yang. Carbon nanofibers (CNFs) supported cobalt-nickel sulfide (CoNi2S4) nanoparticles hybrid anode for high performance lithium ion capacitor. *Scientific Reports*, 8(1):1–11, 2018. ISSN 20452322. doi: 10.1038/s41598-018-19787-z. URL http://dx.doi.org/10.1038/s41598-018-19787-z.

[90] Afeesh Rajan Unnithan, Arathyram Ramachandra Kurup Sasikala, Shalom Sara Thomas, Amin Ghavami Nejad, Youn Soo Cha, Chan Hee Park, and Cheol Sang Kim. Strategic Design and Fabrication of Biomimetic 3D Scaffolds: Unique Architectures of Extracellular Matrices for Enhanced Adipogenesis and Soft Tissue Reconstruction. *Sci-*

entific Reports, 8(1):1–12, 2018. ISSN 20452322. doi: 10.1038/s41598-018-23966-3. URL http://dx.doi.org/10.1038/s41598-018-23966-3.

[91] Longquan Chen and Elmar Bonaccurso. Electrowetting - From statics to dynamics. *Advances in Colloid and Interface Science*, 210:2–12, 2014. ISSN 00018686. doi: 10.1016/j.cis.2013.09.007. URL http://dx.doi.org/10.1016/j.cis.2013.09.007.

[92] Frieder Mugele, Michel Duits, and Dirk Van Den Ende. Electrowetting: A versatile tool for drop manipulation, generation, and characterization. *Advances in Colloid and Interface Science*, 161(1-2):115–123, 2010. ISSN 00018686. doi: 10.1016/j.cis.2009.11.002. URL http://dx.doi.org/10.1016/j.cis.2009.11.002.

[93] Frieder Mugele and Jean Christophe Baret. Electrowetting: From basics to applications. *Journal of Physics Condensed Matter*, 17(28), 2005. ISSN 09538984. doi: 10.1088/0953-8984/17/28/R01.